

Gaussian-Mixture-Model Q-Functions for Policy Iteration in Reinforcement Learning

Minh Vu and Konstantinos Slavakis, *Senior Member, IEEE*

Abstract—Unlike their conventional use as estimators of probability density functions in reinforcement learning (RL), this paper introduces a novel function-approximation role for Gaussian mixture models (GMMs) as direct surrogates for Q-function losses. These parametric models, termed GMM-QFs, possess substantial representational capacity, as they are shown to be universal approximators over a broad class of functions. They are further embedded within Bellman residuals, where their learnable parameters—a fixed number of mixing weights, together with Gaussian mean vectors and covariance matrices—are inferred from data via optimization on a Riemannian manifold. This geometric perspective on the parameter space naturally incorporates Riemannian optimization into the policy-evaluation step of standard policy-iteration frameworks. Rigorous theoretical results are established, and supporting numerical tests show that, even without access to experience data, GMM-QFs deliver competitive performance and, in some cases, outperform state-of-the-art approaches across a range of benchmark RL tasks, all while maintaining a significantly smaller computational footprint than deep-learning methods that rely on experience data.

Index Terms—Reinforcement learning, Gaussian-mixture models, policy iteration, Q-functions, Riemannian optimization.

I. INTRODUCTION

Reinforcement learning (RL) [1, 2] is a machine-learning paradigm in which an intelligent “agent” interacts with its environment to determine an optimal policy that minimizes the cumulative cost/loss associated with its “actions.” Typically, RL models the environment as a Markov decision process (MDP) [1], thereby furnishing a rigorous mathematical framework for addressing arduous sequential decision-making problems that arise in numerous real-world domains, including robotics, wireless communications, data mining, and bioinformatics [1].

To determine an optimal policy, RL strategies generally aim to estimate the value or loss (Q-function) corresponding to the selection of a particular action in a given state, using feedback obtained from the environment (Figure 1). Classical methods such as Q-learning [3] and state-action-reward-state-action (SARSA) [4] estimate Q-functions via lookup tables that store Q-values for every possible state-action pair. Although effective in environments with discrete and small-scale state-action spaces, these tabular approaches become computationally prohibitive in practical settings characterized by continuous or large-scale state-action spaces. To mitigate this limitation, significant attention has been devoted to the development of RL algorithms that leverage (typically non-linear) models to approximate Q-functions [1].

The authors are with the Department of Information and Communications, Institute of Science Tokyo, 4259-G2-4 Nagatsuta-cho, Midoriku, Yokohama, Kanagawa, Japan. Emails: vu.d.a5c3@m.isct.ac.jp, slavakis@ict.eng.isct.ac.jp

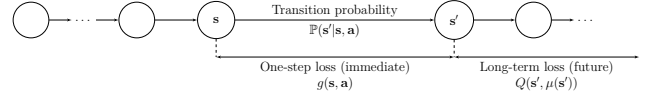


Fig. 1: RL as a sequential decision-making process: at state s , the RL agent takes decision/action $\mathbf{a} := \mu(s)$, suffers the one-step loss $g(s, \mathbf{a})$, and moves to the next state s' according to some transition probability. Function $\mu(\cdot)$ denotes the policy or decision-making mechanism. The agent seeks to identify a policy that minimizes the cumulative (long-term) loss—quantified by the Q-function $Q(\cdot)$ —incurred over its sequence of actions.

Approximation models for Q-functions have a long-standing history in RL. Classical kernel-based (KB)RL methods [5–7] represent Q-functions as elements of Banach spaces, typically those comprising all essentially bounded functions. Methods such as temporal difference (TD) [8], least-squares (LS)TD [9–11], Bellman-residual (BR) approaches [12], and more recent nonparametric designs [13–15] model Q-functions within user-defined reproducing kernel Hilbert spaces (RKHSs) [16, 17], thereby exploiting the underlying geometric structure and computational efficiency afforded by the reproducing inner product. A notable drawback of these kernel-based models, however, is that their number of design parameters typically scales with the quantity of observed data, which can result in significant memory and computational overhead—particularly in dynamic settings with nonstationary data distributions. To alleviate this limitation, dimensionality-reduction techniques have been introduced [11, 13]. Nevertheless, constraining often the number of basis elements in the approximation subspace to effect dimensionality reduction may lead to degraded accuracy in the resulting Q-function estimates. A comprehensive review of KBRL, (LS)TD, and BR methods, along with their connections to RKHSs, is provided in [15].

Deep neural networks have been widely adopted as non-linear Q-function approximators, most notably in the form of deep Q-networks (DQNs), e.g., [18, 19]. These models are typically trained using *experience data* [20] gathered from previously employed policies and stored in a *replay buffer*. The replay buffer serves as a repository of prior knowledge and contributes significantly to stabilizing the training of DQN-based algorithms. While DQNs offer a practical and powerful means of training RL agents—leveraging the computational efficiency and expressiveness of neural networks—they exhibit limitations in several key scenarios. In particular, deployment in an online setting requires swift adaptation to new data, which becomes challenging to DQNs due to the large number of learnable data within the deep networks. Frequent model update with new data (re-training), although theoretically possible within simulation scope, is computationally expensive and requires significant hardware resources, contradicting the

lightweight and rapid adaptability requirements of usual online learning. Moreover, large-scale neural networks in DQNs are notoriously more prone to instability and overfitting, further reducing their robustness when faced with non-stationary or unpredictable real-world conditions (out-of-distribution problems).

In distributional RL [21–25]—a prominent and increasingly influential direction in RL—Q-functions are usually treated as (statistics of) random variables (RVs). For instance, [22] assumes that samples of value or Q-functions are jointly Gaussian, an assumption that, when combined with classical least squares (LS) and Gauss-Markov theory, leads to Kalman-type algorithmic solutions. To enable more expressive probabilistic modeling, Gaussian mixture models (GMMs) [26, 27] have been widely adopted to approximate either the joint PDF $p(Q, \mathbf{s}, \mathbf{a})$ —in which Q-function Q , state \mathbf{s} , and action \mathbf{a} are all modeled as realizations (observations) of RVs—or the conditional $p(Q | \mathbf{s}, \mathbf{a})$. This conventional use of GMMs, closely linked to maximum likelihood estimation [28, 29], naturally motivates the adoption of expectation-maximization (EM) procedures [21–24]. As such, distributional RL estimates a desirable Q *indirectly* as a statistical byproduct of the modeled PDF—most commonly as the mean of the conditional distribution $p(Q | \mathbf{s}, \mathbf{a})$ in EM-based solutions. Nevertheless, it is well-established that EM algorithms are highly sensitive to initialization [29], which can negatively impact convergence and stability.

This manuscript emphasizes the following key contributions.

- (C1) GMMs are employed here *directly* as surrogates for Q-functions, rather than as approximators of PDFs. The proposed GMMs act as universal approximators for a broad class of functions—see Theorem 3. Without imposing any statistical assumptions on Q-function evaluations, GMMs are integrated into a Bellman-residual-inspired loss, wherein the GMM hyperparameters—mixing weights, mean vectors, and covariance matrices—are optimized over a Riemannian manifold. This geometric viewpoint introduces the versatile machinery of Riemannian optimization [30] into the policy-evaluation step of standard policy-iteration schemes. Although both GMMs and Riemannian optimization have previously been utilized to model stochastic policy functions [31]—that is, conditional PDFs—within the framework of policy gradient and policy search methods [32], the direct use of GMMs as Q-function surrogates, trained via Riemannian optimization, appears to be new within the RL literature.
- (C2) The proposed methodology establishes a *parametric* model, in contrast to the nonparametric strategies [33] employed in the popular KBRL [5–12], wherein the number of tunable hyperparameters increases with the volume of observed data. In the parametric GMM-QFs, by contrast, the number of learnable hyperparameters—namely, the mixing weights, mean vectors, and covariance matrices of the Gaussian kernels—remains fixed, regardless of the size of the observed dataset. Numerical tests—see, for instance, Table I—demonstrate that GMM-QFs require fewer hyperparameters to achieve performance

comparable to, and in many cases surpassing, that of standard DQNs. This reduced parameterization footprint fosters a computationally efficient framework and facilitates natural connections with robust-modeling principles.

The manuscript is organized as follows. Section II reviews the classical Bellman mappings and establishes the notation used throughout the paper. The proposed class of GMM-QFs, together with their universal approximation properties, is introduced in Section III. The policy iteration (PI) framework incorporating these models and driven by Riemannian optimization, along with its performance analysis, is detailed in Section IV. Numerical experiments on standard benchmark control tasks are reported in Section V. Finally, Section VI provides concluding remarks and outlines directions for future research. This manuscript also constitutes a substantial extension of the short conference paper [34].

II. POLICY ITERATION AND BELLMAN RESIDUALS

A. Notations

Let $\mathfrak{S} \subset \mathbb{R}^D$ denote the *continuous* state space, with state vector $\mathbf{s} \in \mathfrak{S}$, for some $D \in \mathbb{N}_*$ (\mathbb{N}_* is the set of all positive integers). The *discrete* and *finite* action space is denoted by \mathfrak{A} , with action $\mathbf{a} \in \mathfrak{A}$. An agent, currently at state $\mathbf{s} \in \mathfrak{S}$, takes action $\mathbf{a} \in \mathfrak{A}$ and transits to a new state $\mathbf{s}' \in \mathfrak{S}$ under transition probability $p(\mathbf{s}' | \mathbf{s}, \mathbf{a})$, which is unknown to the user/agent in most cases of practice. This transition is also penalized through a real-valued scalar, termed the *one-step* penalty (loss), which represents the immediate or short-term cost of the agent’s action \mathbf{a} at state \mathbf{s} and is typically provided by the environment; see Figure 1.

For convenience, define also the state-action vector $\mathbf{z} := \zeta(\mathbf{s}, \mathbf{a})$, with a user-defined mapping $\zeta: \mathfrak{S} \times \mathfrak{A} \rightarrow \mathfrak{Z} \subset \mathbb{R}^{D_z}$, where $D_z \in \mathbb{N}_*$. Mapping $\zeta(\cdot, \cdot)$ is introduced to accommodate a broad range of state-action pairs, including cases where the discrete \mathfrak{A} is categorical, e.g., it contains actions such as “move to the left” or “move to the right.” Even when \mathfrak{A} is categorical, the mapping $\zeta(\cdot, \cdot)$ is introduced so that \mathfrak{Z} becomes a subset of the continuous space \mathbb{R}^{D_z} , thereby enabling the subsequent definition of Gaussian functions on \mathfrak{Z} .

As such, \mathfrak{Z} serves as the domain of the *one-step loss* $g: \mathfrak{Z} \rightarrow \mathbb{R}: \mathbf{z} \mapsto g(\mathbf{z})$, as well as of the *Q-function* $Q: \mathfrak{Z} \rightarrow \mathbb{R}: \mathbf{z} \mapsto Q(\mathbf{z})$. Consequently, the one-step penalty received from the environment when the agent takes action \mathbf{a} in state \mathbf{s} is given by $g(\zeta(\mathbf{s}, \mathbf{a})) \in \mathbb{R}$, while $Q(\zeta(\mathbf{s}, \mathbf{a}))$ represents the *long-term* cost that the agent will incur over an infinite future horizon if it takes action \mathbf{a} in state \mathbf{s} ; see Figure 1. The exact functional forms of g and Q are typically unknown to the agent, but are commonly modeled and inferred from observed data together with a-priori knowledge of the surrounding environment.

Following [1], consider the set of all mappings $\mathcal{M} := \{\mu(\cdot) | \mu(\cdot): \mathfrak{S} \rightarrow \mathfrak{A}: \mathbf{s} \mapsto \mu(\mathbf{s})\}$. In other words, $\mu(\mathbf{s})$ denotes the action that the agent takes at state \mathbf{s} under μ . The set of policies is defined as $\Pi := \mathcal{M}^{\mathbb{N}} := \{\mu_0, \mu_1, \dots, \mu_n, \dots | \mu_n \in \mathcal{M}, n \in \mathbb{N}\}$. A policy will be denoted by $\pi \in \Pi$. Given $\mu \in \mathcal{M}$, a stationary policy π_μ is defined as $\pi_\mu := (\mu, \mu, \dots, \mu, \dots)$. It is customary for μ to denote also π_μ . Finally, for compact notations, let $\bar{1}, \bar{K} := \{1, \dots, K\}$, for any $K \in \mathbb{N}_*$.

B. Bellman mappings, policy iteration, and approximation spaces

The classical *Bellman mappings* [1] compute the total cost—that is, the sum of the one-step loss and the expected long-term loss—the agent would incur if action \mathbf{a} were taken at state \mathbf{s} . More specifically, if \mathcal{B} stands for a *user-defined* space of Q-functions, typically taken as the Banach space of all essentially bounded functions [1], then the classical Bellman mappings $\mathcal{T}_\mu^\diamond, \mathcal{T}^\diamond: \mathcal{B} \rightarrow \mathcal{B}: Q \mapsto \mathcal{T}_\mu^\diamond Q, \mathcal{T}^\diamond Q$ are defined as [1]

$$(\mathcal{T}_\mu^\diamond Q)(\zeta(\mathbf{s}, \mathbf{a})) := g(\zeta(\mathbf{s}, \mathbf{a})) + \alpha \mathbb{E}_{s'|(\mathbf{s}, \mathbf{a})} \{Q(\zeta(\mathbf{s}', \mu(\mathbf{s}')))\}, \quad (1a)$$

$$(\mathcal{T}^\diamond Q)(\zeta(\mathbf{s}, \mathbf{a})) := g(\zeta(\mathbf{s}, \mathbf{a})) + \alpha \mathbb{E}_{s'|(\mathbf{s}, \mathbf{a})} \left\{ \min_{\mathbf{a}' \in \mathfrak{A}} Q(\zeta(\mathbf{s}', \mathbf{a}')) \right\}, \quad (1b)$$

$\forall(\mathbf{s}, \mathbf{a})$, where $\mathbb{E}_{s'|(\mathbf{s}, \mathbf{a})} \{\cdot\}$ stands for the conditional expectation operator with respect to (w.r.t.) the potentially next state \mathbf{s}' conditioned on (\mathbf{s}, \mathbf{a}) , and $\alpha \in [0, 1)$ is the discount factor. A more rigorous discussion based on probabilistic arguments and notation is deferred to Section IV-C. Mapping (1a) refers to the case where the agent takes actions according to a stationary policy μ , while (1b) serves as a greedy variation of (1a).

For a mapping $\mathcal{T}: \mathcal{B} \rightarrow \mathcal{B}$, its fixed-point set is defined as $\text{Fix } \mathcal{T} := \{Q \in \mathcal{B} \mid \mathcal{T}Q = Q\}$. It is well-known that $\text{Fix } \mathcal{T}_\mu^\diamond$ and $\text{Fix } \mathcal{T}^\diamond$ play central roles in identifying *optimal* policies which minimize the total loss [1]. Usually, the discount factor $\alpha \in [0, 1)$ to render $\mathcal{T}_\mu^\diamond, \mathcal{T}^\diamond$ strict contractions and to ensure that $\text{Fix } \mathcal{T}_\mu^\diamond$ and $\text{Fix } \mathcal{T}^\diamond$ are nonempty and singletons [1, 35]. These arguments will be revisited in Section IV-C.

Policy iteration (PI) is a popular RL framework [1, 2]. It comprises two stages per iteration $n \in \mathbb{N}$: *policy evaluation* and *policy improvement*; see Figure 2. For example, given a stationary policy μ_n at iteration n , policy evaluation computes a Q-function Q_n that “closely” approximates, in an appropriate sense—when possible— $Q_{\mu_n}^\diamond \in \text{Fix } \mathcal{T}_{\mu_n}^\diamond$, while policy improvement updates the policy according to the following greedy rule:

$$\mu_{n+1}(\mathbf{s}) := \arg \min_{\mathbf{a} \in \mathfrak{A}} Q_n(\zeta(\mathbf{s}, \mathbf{a})), \quad \forall \mathbf{s} \in \mathfrak{S}. \quad (2)$$

PI repeats this process to generate a sequence of (stationary) policies and Q-functions as in $\mu_0 \rightarrow Q_0 \rightarrow \mu_1 \rightarrow Q_1 \rightarrow \dots$ (Figure 2), with the goal that the resulting sequence of the Q-functions converges, in some sense, to $Q^\diamond \in \text{Fix } \mathcal{T}^\diamond$. The *optimal policy* then is defined as $\mu^\diamond(\mathbf{s}) := \arg \min_{\mathbf{a} \in \mathfrak{A}} Q^\diamond(\zeta(\mathbf{s}, \mathbf{a})), \forall \mathbf{s}$.

Real-world problems involving high-dimensional or even continuous state spaces \mathfrak{S} pose significant computational challenges for tabular methods, where Q-functions must be evaluated at *every* $\mathbf{s} \in \mathfrak{S}$ to identify policies—see, for example, (2). To address this limitation, function-approximation models for Q-functions have been developed as viable alternatives to tabular methods, enabling *approximate PI* schemes through their incorporation into policy-evaluation steps.

To this end, a reproducing kernel Hilbert space (RKHS) \mathcal{H} is a popular choice for the underlying approximation space

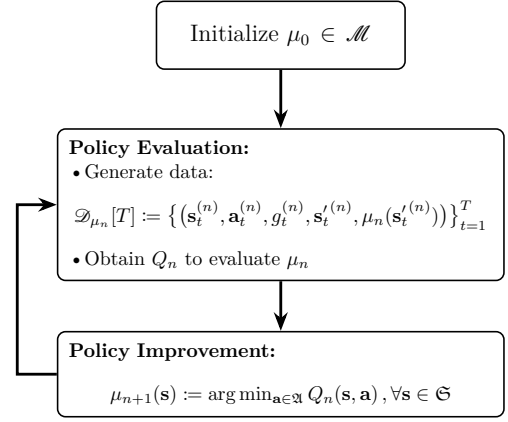


Fig. 2: Policy iteration consists of two steps: policy evaluation and policy improvement. The “exploration” dataset $\mathcal{D}_{\mu_n}[T]$ is collected on the fly under the current policy μ_n and is distinct from experience data, which are gathered under previous policies and stored in a replay buffer. The proposed framework (Algorithm 1) relies exclusively on $\mathcal{D}_{\mu_n}[T]$ and does *not* use any experience data or a replay buffer.

of Q-functions [5–15], owing to the presence of an inner product and the reproducing property induced by its associated kernel [16, 17]—features that are absent in a Banach space, which is the typical choice for \mathcal{B} in the earlier discussion. For an RKHS \mathcal{H} and its inner product $\langle \cdot | \cdot \rangle_{\mathcal{H}}$, induced by a reproducing kernel $\kappa(\cdot, \cdot): \mathbb{R}^{D_z} \times \mathbb{R}^{D_z} \rightarrow \mathbb{R}: (\mathbf{z}', \mathbf{z}) \mapsto \kappa(\mathbf{z}', \mathbf{z})$ [16, 17], with the feature mapping $\varphi(\cdot): \mathbb{R}^{D_z} \rightarrow \mathcal{H}: \mathbf{z} \mapsto \varphi(\mathbf{z}) := \kappa(\cdot, \mathbf{z})$. A popular RKHS example is the space $\mathcal{H}_{\mathbf{C}}$, induced by the following Gaussian kernel

$$\kappa(\mathbf{z}', \mathbf{z}) := \mathcal{G}(\mathbf{z}' | \mathbf{z}, \mathbf{C}) := e^{-(\mathbf{z}' - \mathbf{z})^\top \mathbf{C}^{-1} (\mathbf{z}' - \mathbf{z})}, \quad (3)$$

for an arbitrarily fixed matrix \mathbf{C} in the set of all $D_z \times D_z$ positive definite matrices $\mathbb{S}_{++}^{D_z}$. In this case, the feature mapping becomes $\varphi(\mathbf{z}) = \mathcal{G}(\cdot | \mathbf{z}, \mathbf{C})$, and

$$\mathcal{H}_{\mathbf{C}}^{\text{pre}} := \left\{ \sum_{k=1}^K \xi_k \mathcal{G}(\cdot | \mathbf{z}_k, \mathbf{C}) \mid \{\xi_k\}_{k=1}^K \subset \mathbb{R}, \{\mathbf{z}_k\}_{k=1}^K \subset \mathbb{R}^{D_z}, K \in \mathbb{N}_* \right\}, \quad (4a)$$

$$\mathcal{H}_{\mathbf{C}} := \text{clos } \mathcal{H}_{\mathbf{C}}^{\text{pre}}, \quad (4b)$$

where (4a) is a pre-Hilbert space, while (4b) completes that space by the closure clos , taken w.r.t. the topology arising from the inner product induced by (3).

C. Bellman residuals

Due to the lack of knowledge on transition probabilities in most cases of practice, the computation of the conditional expectation in (1a) becomes infeasible. To surmount this limitation, RL studies usually consider a sampling dataset $\mathcal{D}_\mu[T] := \{(s_t, \mathbf{a}_t := \mu(s_t), g_t := g(\zeta(s_t, \mathbf{a}_t)), s_t')\}_{t=1}^T \subset \mathfrak{S} \times \mathfrak{A} \times \mathfrak{S} \times \mathbb{R}$, for a stationary $\mu(\cdot)$ and a usually large $T \in \mathbb{N}_*$. Here, s_t' denotes the successor state of s_t , if action \mathbf{a}_t is taken under policy $\mu(\cdot)$. For convenience in notations, let $\mathbf{z}_t := \zeta(s_t, \mathbf{a}_t)$ and $\mathbf{z}_t' := \zeta(s_t', \mu(s_t'))$.

Lacking access to the conditional expectation, rather than relying on the ensemble-based formulation in (1a), the Bellman

residual (BR) approach [12, 15, 36] computes the following *empirical* Bellman mapping:

$$\hat{\mathcal{T}}_\mu Q := \arg \min_{Q' \in \mathcal{H}} \overbrace{\frac{1}{T} \sum_{t=1}^T [g_t + \alpha Q'(\mathbf{z}_t) - Q'(\mathbf{z}_t)]^2}^{\hat{\mathcal{L}}_\mu[T](Q')} + \rho \|Q' - Q\|_{\mathcal{H}}^2, \quad (5)$$

where ρ is a regularization coefficient, introduced to stabilize solutions along the lines of the celebrated Tikhonov regularization. The *empirical* loss $\hat{\mathcal{L}}_\mu[T](\cdot)$ serves as an estimate of the *ensemble* one:

$$\mathcal{L}_\mu(Q) := \mathbb{E}\{[g(\mathbf{z}) + \alpha Q(\mathbf{z}') - Q(\mathbf{z})]^2\}, \quad (6)$$

where $\mathbb{E}\{\cdot\}$ stands for expectation—a rigorous probabilistic discussion is deferred to Section IV-C.

RKHSs have been already widely employed not only in BR schemes but also in temporal-difference (TD) learning, via gradient-descent-based solutions [8, 12], as well as in least-squares (LS)TD [9–11]. Owing to the representer theorem [17, 37], all admissible Q-functions in an RKHS are expressed as elements of the linear subspace of \mathcal{H} spanned by $\{\varphi(\mathbf{z}_t), \varphi(\mathbf{z}'_t)\}_{t=1}^T$. However, this property is precisely the source of the “curse of dimensionality” in RKHS-based nonparametric methods [5–15]: increasing the representational capacity of $\{\varphi(\mathbf{z}_t), \varphi(\mathbf{z}'_t)\}_{t=1}^T$ requires a large number T of data samples, which enhances expressiveness but simultaneously impairs computational efficiency due to the resulting increase in complexity. A comprehensive variational framework for nonparametric solutions via RKHSs, encompassing (LS)TD and BR solutions, is presented in [15].

III. THE CLASS OF GMM Q-FUNCTIONS (GMM-QFs)

A. Definition of GMM-QFs

Selecting an “optimal” kernel function in (4)—through the choice of the matrix \mathbf{C} —to fit the data requires substantial manual effort and poses a significant challenge in RKHS-based nonparametric methods [5–15]. This difficulty persists even when multiple kernels are employed. Unfortunately, the need for careful kernel selection further exacerbates the notorious “curse of dimensionality” in nonparametric designs, discussed at the end of Section II-C.

To mitigate these shortcomings of nonparametric designs, this paper introduces a novel *parametric* functional approximation model for Q-functions. Motivated by GMMs [27], and for a user-defined $K \in \mathbb{N}_*$, GMM-QFs are defined as the following class of functionals:

$$\mathcal{Q}_K := \left\{ Q(\cdot) := \sum_{k=1}^K \xi_k \mathcal{G}_k(\cdot \mid \mathbf{m}_k, \mathbf{C}_k) \mid \{\xi_k\}_{k=1}^K \subset \mathbb{R}, \right. \\ \left. \{\mathbf{m}_k\}_{k=1}^K \subset \mathbb{R}^{D_z}, \{\mathbf{C}_k\}_{k=1}^K \subset \mathbb{S}_{++}^{D_z} \right\}, \quad (7)$$

where the function $\mathcal{G}_k(\cdot) := \mathcal{G}(\cdot \mid \mathbf{m}_k, \mathbf{C}_k)$ is defined by (3), with the symbol \mathbf{m}_k used instead of \mathbf{z} to underline the fact that \mathbf{m}_k serves as the “mean” of the Gaussian \mathcal{G}_k . Notice also that $\mathcal{Q}_K \subset \mathcal{Q}_{K+1}$, $\forall K \in \mathbb{N}_*$, so that $\bigcup_{k=1}^K \mathcal{Q}_k = \mathcal{Q}_K$.

Without any loss of generality, no two \mathcal{G}_k s in the Q-function representation of (7) are considered to be identical, that is,

$(\mathbf{m}_k, \mathbf{C}_k) \neq (\mathbf{m}_{k'}, \mathbf{C}_{k'}), \forall (k, k') \in \overline{1, K^2}$. This is justified by the fact that two or more \mathcal{G}_k s with common $(\mathbf{m}_k, \mathbf{C}_k)$ can be consolidated into a single one with an aggregated mixing weight ξ_k . Actually, the following Theorem 1 has more to say about the Q-function representation in (7).

Theorem 1. Consider $\{\mathbf{C}_k\}_{k=1}^K \subset \mathbb{S}_{++}^{D_z}$, with $\mathbf{C}_k \neq \mathbf{C}_{k'}$, $\forall k \neq k'$. Let $\sum_{k=1}^K \beta_k Q_k = 0$, for some $\{\beta_k\}_{k=1}^K \subset \mathbb{R}$, where $Q_k \in \mathcal{H}_{\mathbf{C}_k}^{\text{pre}} \setminus \{0\}$, $\forall k \in \overline{1, K}$, and $\mathcal{H}_{\mathbf{C}_k}^{\text{pre}}$ is defined by (4a). Then, $\beta_k = 0$, $\forall k \in \overline{1, K}$. Consequently, $\sum_{k=1}^K \mathcal{H}_{\mathbf{C}_k}^{\text{pre}}$ turns out to be the direct sum $\bigoplus_{k=1}^K \mathcal{H}_{\mathbf{C}_k}^{\text{pre}}$.

Proof. See Appendix A. \square

Theorem 1 suggests that any Q-function Q in $\sum_{k=1}^K \mathcal{H}_{\mathbf{C}_k}^{\text{pre}}$, and certainly in its subset \mathcal{Q}_K , has a *unique* representation $Q = \sum_{k=1}^K \xi_k Q_k$, where $\xi_k \in \mathbb{R}$ and each $Q_k \in \mathcal{H}_{\mathbf{C}_k}^{\text{pre}}, \forall k \in \overline{1, K}$.

The mixing weights $\{\xi_k\}_{k=1}^K$ in (7) are not subject to any constraints, unlike in distributional RL, where GMMs model PDFs and the mixing weights must be chosen so that $\int Q(\mathbf{z}) d\mathbf{z} = 1$ [21–25]. Moreover, in contrast to nonparametric approaches [5–15], where $\{\mathbf{m}_k, \mathbf{C}_k\}_{k=1}^K$ are determined by the observed data and only $\{\xi_k\}_{k=1}^K$ are treated as learnable parameters, GMM-QFs consider $\{\mathbf{m}_k, \mathbf{C}_k\}_{k=1}^K$ as learnable as well. The functional representation in (7) is also referred to in the literature as radial-basis-function (RBF) [33] or elliptic-basis-function (EBF) networks [38].

Motivated by (7), define the following parameter space:

$$\mathfrak{M}_K := \left\{ \Omega := (\xi_1, \dots, \xi_K, \mathbf{m}_1, \dots, \mathbf{m}_K, \mathbf{C}_1, \dots, \mathbf{C}_K) \mid \right. \\ \left. \xi_k \in \mathbb{R}, \mathbf{m}_k \in \mathbb{R}^{D_z}, \mathbf{C}_k \in \mathbb{S}_{++}^{D_z}, \forall k \in \overline{1, K} \right\} \\ = \mathbb{R}^K \times (\mathbb{R}^{D_z})^K \times (\mathbb{S}_{++}^{D_z})^K. \quad (8)$$

The mapping

$$\mathcal{P}(\cdot): \mathfrak{M}_K \rightarrow \mathcal{Q}_K: \Omega \mapsto \sum_{k=1}^K \xi_k \mathcal{G}_k(\cdot \mid \mathbf{m}_k, \mathbf{C}_k), \quad (9)$$

is clearly surjective. For any Q-function $Q \in \mathcal{Q}_K$, the pre-image $\mathcal{P}^{-1}(Q)$ is non-empty because $\mathcal{P}(\cdot)$ is surjective, though it may not be a singleton. For example, when $K = 2$, parameter tuples $\Omega := (\xi_1, \xi_2, \mathbf{m}, \mathbf{m}, \mathbf{C}, \mathbf{C})$ and $\Omega' := (\xi_1 + \xi_2, 0, \mathbf{m}, \mathbf{m}, \mathbf{C}, \mathbf{C})$ are both mapped to the same Q-function under $\mathcal{P}(\cdot)$. Therefore, if $\mathcal{P}^{-1}(Q)$ is regarded as a single “element”—more precisely, by introducing an equivalence relation such that (s.t.) $\mathcal{P}^{-1}(Q)$ forms an equivalence class in the quotient space \mathfrak{M}_K —then mapping $\mathcal{P}(\cdot)$, which maps equivalence classes to Q-functions, can be also viewed as one-to-one, and hence bijective.

Interestingly, being the Cartesian product of well-known Riemannian manifolds in (8), \mathfrak{M}_K is itself Riemannian [39]. Exploitation of the geometric structure of Riemannian manifold of parameters constitutes a key objective of this work and will be discussed in depth in Section IV.

B. Representational capacity of GMM-QFs

The following assumption is commonly adopted in theoretical studies of RL, e.g., [11], and is motivated by practical

hardware constraints, as sensors in real-world devices can only measure physical quantities within finite operating ranges.

Assumption 2. The state-action space \mathfrak{Z} is a compact subset of \mathbb{R}^{D_z} .

The following theorem establishes that the proposed GMM-QFs in (7) possess sufficient representational capacity to approximate broad families of functions.

Theorem 3 (Universal-approximation properties of GMM-QFs).

- (i) Under Assumption 2, the set $\cup_{K \in \mathbb{N}_*} \mathcal{Q}_K$ is dense in the Banach space $C(\mathfrak{Z})$ of all real-valued continuous functions defined on \mathfrak{Z} , equipped with the sup-norm $\|\cdot\|_\infty$. In other words, for any $Q \in C(\mathfrak{Z})$ and for any $\varepsilon \in \mathbb{R}_{++}$, there exist a $K \in \mathbb{N}_*$ and a $\tilde{Q} \in \mathcal{Q}_K$ s.t.

$$\|Q - \tilde{Q}\|_\infty := \sup_{\mathbf{z} \in \mathfrak{Z}} |Q(\mathbf{z}) - \tilde{Q}(\mathbf{z})| \leq \varepsilon. \quad (10)$$

- (ii) Under Assumption 2, $\cup_{K \in \mathbb{N}_*} \mathcal{Q}_K$ is dense in the Hilbert space $L_2(\mathfrak{P}) := L_2(\mathfrak{Z}, \mathfrak{B}(\mathfrak{Z}), \mathfrak{P})$ of all real-valued square-integrable functionals on \mathfrak{Z} w.r.t. the probability space $(\mathfrak{Z}, \mathfrak{B}(\mathfrak{Z}), \mathfrak{P})$, where $\mathfrak{B}(\mathfrak{Z})$ is a Borel σ -algebra on \mathfrak{Z} and \mathfrak{P} is a probability measure on $\mathfrak{B}(\mathfrak{Z})$ [40–42]. In other words, for any $Q \in L_2(\mathfrak{P})$ and for any $\varepsilon \in \mathbb{R}_{++}$, there exist a $K \in \mathbb{N}_*$ and a $\tilde{Q} \in \mathcal{Q}_K$ s.t.

$$\begin{aligned} \|Q - \tilde{Q}\|_{L_2(\mathfrak{P})} &:= \left(\int_{\mathfrak{Z}} |Q(\mathbf{z}) - \tilde{Q}(\mathbf{z})|^2 \mathfrak{P}(d\mathbf{z}) \right)^{\frac{1}{2}} \\ &:= (\mathbb{E}\{|Q(\cdot) - \tilde{Q}(\cdot)|^2\})^{\frac{1}{2}} \leq \varepsilon, \end{aligned} \quad (11)$$

where $\mathbb{E}\{\cdot\}$ denotes expectation, defined as the integral w.r.t. \mathfrak{P} .

- (iii) In the case where \mathfrak{Z} becomes the non-compact \mathbb{R}^{D_z} , $\cup_{K \in \mathbb{N}_*} \mathcal{Q}_K$ is dense in the Hilbert space $L_2(\mathbb{R}^{D_z})$ of all real-valued square-integrable functionals on \mathbb{R}^{D_z} w.r.t. the classical Lebesgue measure [40–42]. In other words, for any $Q \in L_2(\mathbb{R}^{D_z})$ and for any $\varepsilon \in \mathbb{R}_{++}$, there exist a $K \in \mathbb{N}_*$ and a $\tilde{Q} \in \mathcal{Q}_K$ s.t.

$$\|Q - \tilde{Q}\|_{L_2(\mathbb{R}^{D_z})} := \left(\int_{\mathbb{R}^{D_z}} |Q(\mathbf{z}) - \tilde{Q}(\mathbf{z})|^2 d\mathbf{z} \right)^{\frac{1}{2}} \leq \varepsilon. \quad (12)$$

Proof. See Appendix B. \square

A similar result to Theorem 3(iii) is presented in [33], where it is shown that RBF networks with *diagonal* covariance matrices are dense in the spaces $L_p(\mathbb{R}^{D_z})$, $p \in \mathbb{N}_*$. Theorem 3(iii) extends the result of [33] to general non-diagonal covariance matrices for the case of $L_2(\mathbb{R}^{D_z})$.

Motivated by Theorem 3(i), the following proposition shows that it is sufficient to search within the class of GMM-QFs, $\cup_{K \in \mathbb{N}_*} \mathcal{Q}_K$, for a minimizer of the empirical loss $\hat{\mathcal{L}}_\mu[T](\cdot)$ defined in (5), rather than over the broader class of Q-functions $C(\mathfrak{Z})$.

Proposition 4. Under Assumption 2,

$$\inf_{Q \in C(\mathfrak{Z})} \hat{\mathcal{L}}_\mu[T](Q) = \inf_{Q \in \cup_{K \in \mathbb{N}_*} \mathcal{Q}_K} \hat{\mathcal{L}}_\mu[T](Q).$$

Proof. See Appendix C. \square

Guided by Theorem 3 and Proposition 4, and the discussion on (9), the subsequent search for suitable GMM-QFs will be conducted over the Riemannian parameter space \mathfrak{M}_K defined in (8), for a sufficiently large value of K .

IV. POLICY ITERATION BY RIEMANNIAN OPTIMIZATION

Based on (8) and the accompanying discussion, the empirical loss $\hat{\mathcal{L}}_\mu[T](\cdot)$ of (5) is minimized over the parameter space \mathfrak{M}_K for a fixed user-defined K —a Riemannian manifold according to the discussion at the end of Section III-A—as follows:

$$\min_{\Omega \in \mathfrak{M}_K} \left(\hat{\mathcal{L}}_\mu[T](\Omega) := \frac{1}{T} \sum_{t=1}^T \left[g_t + \alpha \sum_{k=1}^K \xi_k \mathcal{G}_k(\mathbf{z}'_t) - \sum_{k=1}^K \xi_k \mathcal{G}_k(\mathbf{z}_t) \right]^2 \right), \quad (13)$$

where $\mathcal{G}_k(\cdot) := \mathcal{G}(\cdot | \mathbf{m}_k, \mathbf{C}_k)$ is defined in (3), while $\mathbf{z}_t := \zeta(\mathbf{s}_t, \mathbf{a}_t)$ and $\mathbf{z}'_t := \zeta(\mathbf{s}'_t, \mu(\mathbf{s}'_t))$. Task (13), addressed through Algorithm 2, is integrated into the policy-evaluation stage (line 4) of the PI Algorithm 1—apparently for the first time in the RL literature.

The remainder of this section delves into the details of the Riemannian optimization task (13). To set the stage, several fundamental concepts from Riemannian geometry are first reviewed.

A. Preliminaries on Riemannian manifolds

Loosely speaking, a (*smooth*) *manifold* \mathfrak{M} is a topological space such that any point $\Omega \in \mathfrak{M}$ has a neighborhood that is homeomorphic to an open subset of a Euclidean space [39, §2.8.1]. A tangent vector of \mathfrak{M} at Ω is the “velocity” $\dot{\gamma}(0)$ of a curve $\gamma: \mathbb{R} \rightarrow \mathfrak{M}: t \mapsto \gamma(t)$, where $\gamma(0) = \Omega$ [39, Def. 2.8.17]. The *tangent space* $T_\Omega \mathfrak{M}$ of \mathfrak{M} at Ω is the linear vector space of all tangent vectors of \mathfrak{M} at Ω [39, Def. 2.8.14]. The *retraction* mapping R on \mathfrak{M} is a smooth mapping from the tangent bundle $T\mathfrak{M}$ —the collection of all tangent spaces of \mathfrak{M} —to \mathfrak{M} itself s.t. specific properties hold true [30, Def. 4.1.1]. The restriction of R to $T_\Omega \mathfrak{M}$ is denoted by R_Ω .

A Riemannian manifold \mathfrak{M} is a smooth manifold equipped with a Riemannian metric, that is, a collection of inner products $\langle \cdot | \cdot \rangle_\Omega$, one for every $\Omega \in \mathfrak{M}$ and defined on pairs of tangent vectors in $T_\Omega \mathfrak{M}$, s.t. it induces a specific smooth map for every pair of vector fields on \mathfrak{M} [39, Def. 3.7.1]. The metric naturally defines the norm $\|\cdot\|_\Omega := \langle \cdot | \cdot \rangle_\Omega^{1/2}$. For a Riemannian manifold, its most celebrated retraction is its *exponential* map [30, 39]. Further details on Riemannian geometry fall outside the scope of this study; the interested reader is referred to [30, 39].

Example 5 ([30]). The Euclidean space \mathbb{R}^K is a Riemannian manifold with $T_\xi \mathbb{R}^K = \mathbb{R}^K$, $\forall \xi \in \mathbb{R}^K$, and with Riemannian metric $\langle \theta_1 | \theta_2 \rangle_\xi := \theta_1^\top \theta_2$, $\forall (\theta_1, \theta_2, \xi) \in (\mathbb{R}^K)^3$. The mapping $R_\xi(\theta) := \xi + \theta$, $\forall (\theta, \xi) \in (\mathbb{R}^K)^2$, serves as a retraction on \mathbb{R}^K .

Example 6 ([39, §6.5.3]). The set of all positive-definite matrices $\mathbb{S}_{++}^{D_z}$ is a Riemannian manifold, with $T_{\mathbf{C}} \mathbb{S}_{++}^{D_z} =$

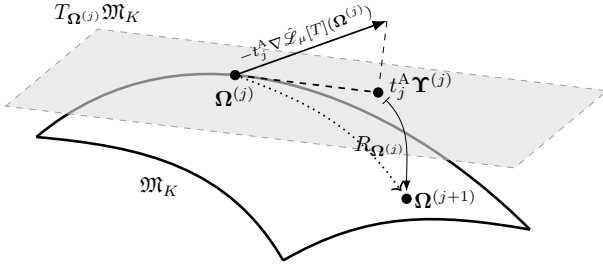


Fig. 3: Gradient of the loss $\hat{\mathcal{L}}_\mu[T](\cdot)$ at $\Omega^{(j)}$, with t_j^A being the (Armijo) step-size. In general, the gradient is first projected onto the tangent space $T_{\Omega^{(j)}}\mathfrak{M}_K$ and then retracted back to the manifold \mathfrak{M}_K . In the present case, however, this projection is unnecessary because, as shown in Proposition 7, the computed gradient already lies in the tangent space.

$\{\Gamma \in \mathbb{R}^{D_z \times D_z} \mid \Gamma^\top = \Gamma\} =: \mathbb{S}^{D_z}$, $\forall \mathbf{C} \in \mathbb{S}_{++}^{D_z}$. The most popular metric is the affine invariant (AffI) one [39, (6.5.11)]: $\forall \mathbf{C} \in \mathbb{S}_{++}^{D_z}$, $\forall (\Gamma_1, \Gamma_2) \in (T_{\mathbf{C}}\mathbb{S}_{++}^{D_z})^2$,

$$\langle \Gamma_1 \mid \Gamma_2 \rangle_{\mathbf{C}}^{\text{AffI}} := \text{tr}(\mathbf{C}^{-1}\Gamma_1\mathbf{C}^{-1}\Gamma_2), \quad (14)$$

where $\text{tr}(\cdot)$ denotes the trace of a square matrix.

Another option for the Riemannian metric is the Bures-Wasserstein (BW) one [43], $\forall \mathbf{C} \in \mathbb{S}_{++}^{D_z}$, $\forall (\Gamma_1, \Gamma_2) \in (T_{\mathbf{C}}\mathbb{S}_{++}^{D_z})^2$,

$$\langle \Gamma_1 \mid \Gamma_2 \rangle_{\mathbf{C}}^{\text{BW}} := \frac{1}{2} \text{tr}(L_{\mathbf{C}}(\Gamma_1)\Gamma_2), \quad (15)$$

where $L_{\mathbf{C}}(\cdot)$ is the Lyapunov operator, with $L_{\mathbf{C}}(\Gamma)$ defined as the solution of $\mathbf{C}L_{\mathbf{C}}(\Gamma) + L_{\mathbf{C}}(\Gamma)\mathbf{C} = \Gamma$, $\forall \Gamma \in T_{\mathbf{C}}\mathbb{S}_{++}^{D_z}$ [44].

The exponential maps $\exp_{\mathbf{C}}(\cdot): T_{\mathbf{C}}\mathbb{S}_{++}^{D_z} \rightarrow \mathbb{S}_{++}^{D_z}: \Gamma \mapsto \exp_{\mathbf{C}}(\Gamma)$ under the AffI and BW metrics are defined as follows [39, (6.5.18)], [43]: $\forall \mathbf{C} \in \mathbb{S}_{++}^{D_z}$, $\forall \Gamma \in T_{\mathbf{C}}\mathbb{S}_{++}^{D_z}$,

$$\exp_{\mathbf{C}}^{\text{AffI}}(\Gamma) := \mathbf{C}^{1/2} \exp(\mathbf{C}^{-1/2}\Gamma\mathbf{C}^{-1/2}) \mathbf{C}^{1/2}, \quad (16a)$$

$$\exp_{\mathbf{C}}^{\text{BW}}(\Gamma) := (L_{\mathbf{C}}(\Gamma) + \mathbf{I}_{D_z}) \mathbf{C} (L_{\mathbf{C}}(\Gamma) + \mathbf{I}_{D_z}), \quad (16b)$$

where $\exp(\cdot)$ stands for the classical exponential matrix [39, §2.5.2], and \mathbf{I}_{D_z} is the $D_z \times D_z$ identity matrix.

B. Algorithms

Notice that for the Riemannian manifold \mathfrak{M}_K , its tangent space at a point $\Omega := (\boldsymbol{\xi}, \mathbf{m}_1, \dots, \mathbf{m}_K, \mathbf{C}_1, \dots, \mathbf{C}_K) \in \mathfrak{M}_K$ becomes $T_{\Omega}\mathfrak{M}_K = T_{\boldsymbol{\xi}}\mathbb{R}^K \times T_{\mathbf{m}_1}\mathbb{R}^{D_z} \times \dots \times T_{\mathbf{m}_K}\mathbb{R}^{D_z} \times T_{\mathbf{C}_1}\mathbb{S}_{++}^{D_z} \times \dots \times T_{\mathbf{C}_K}\mathbb{S}_{++}^{D_z} = \mathbb{R}^K \times (\mathbb{R}^{D_z})^K \times (\mathbb{S}^{D_z})^K$, where it is reminded here that \mathbb{S}^{D_z} stands for the set of all $D_z \times D_z$ symmetric matrices. To run computations on \mathfrak{M}_K , the following straightforward metric is adopted: $\forall \Upsilon_i := (\boldsymbol{\theta}_i, \boldsymbol{\mu}_{i1}, \dots, \boldsymbol{\mu}_{iK}, \Gamma_{i1}, \dots, \Gamma_{iK}) \in T_{\Omega}\mathfrak{M}_K$, $i \in \overline{1, 2}$,

$$\begin{aligned} \langle \Upsilon_1 \mid \Upsilon_2 \rangle_{\Omega} &:= \boldsymbol{\theta}_1^\top \boldsymbol{\theta}_2 + \sum_{k=1}^K \boldsymbol{\mu}_{1k}^\top \boldsymbol{\mu}_{2k} \\ &+ \sum_{k=1}^K \langle \Gamma_{1k} \mid \Gamma_{2k} \rangle_{\mathbf{C}_k}, \end{aligned} \quad (17)$$

where $\langle \cdot \mid \cdot \rangle_{\mathbf{C}_k}$ can be any user-defined Riemannian metric on $\mathbb{S}_{++}^{D_z}$. Here, the AffI and BW metrics, given in (14) and (15), respectively, will serve as the basis for computations.

The solution to (13) relies on a standard steepest-gradient-descent scheme with an Armijo-type line search [30, §4.6.3],

Algorithm 1 Policy iteration by Riemannian optimization

- 1: Arbitrarily initialize $\Omega_0 \in \mathfrak{M}_K$, $\mu_1 \in \mathcal{M}$.
- 2: **while** $n \in \mathbb{N}_*$ **do**
- 3: **Policy evaluation** Use the current policy μ_n to generate the dataset $\mathcal{D}_{\mu_n}[T] := \{(\mathbf{s}_t^{(n)}, \mathbf{a}_t^{(n)}, g_t^{(n)}, \mathbf{s}_t'^{(n)})\}_{t=1}^T$.
- 4: Update Ω_n via Algorithm 2.
- 5: Given Ω_n , compute $Q_n \in \mathcal{Q}_K$ via (7).
- 6: **Policy improvement** Update policy μ_{n+1} via (2).
- 7: Increase n by one, go to Algorithm 1.
- 8: **end while**

Algorithm 2 Solving (13)

- 1: **Require:** Parameters $\bar{\alpha} \in \mathbb{R}_{++}$, $(\beta, \sigma_A) \in (0, 1)^2$, and the number of steps $J \in \mathbb{N}_*$.
- 2: $\Omega^{(0)} := \Omega_{n-1}$.
- 3: **for** $j = 0$ to $J - 1$ **do**
- 4: $\Omega^{(j)} := (\boldsymbol{\xi}^{(j)}, \mathbf{m}_1^{(j)}, \dots, \mathbf{m}_K^{(j)}, \mathbf{C}_1^{(j)}, \dots, \mathbf{C}_K^{(j)})$.
- 5: Use Proposition 7 to compute:

$$\begin{aligned} \nabla \hat{\mathcal{L}}_{\mu_n}[T](\Omega^{(j)}) &= \left(\frac{\partial \hat{\mathcal{L}}_{\mu_n}[T]}{\partial \boldsymbol{\xi}}(\Omega^{(j)}), \dots, \frac{\partial \hat{\mathcal{L}}_{\mu_n}[T]}{\partial \mathbf{m}_k}(\Omega^{(j)}), \right. \\ &\quad \left. \dots, \frac{\partial \hat{\mathcal{L}}_{\mu_n}[T]}{\partial \mathbf{C}_k}(\Omega^{(j)}), \dots \right). \end{aligned}$$

- 6: Let

$$\begin{aligned} \Upsilon^{(j)} &:= (\boldsymbol{\theta}^{(j)}, \boldsymbol{\mu}_1^{(j)}, \dots, \boldsymbol{\mu}_K^{(j)}, \Gamma_1^{(j)}, \dots, \Gamma_K^{(j)}) \\ &:= -\nabla \hat{\mathcal{L}}_{\mu_n}[T](\Omega^{(j)}). \end{aligned}$$

- 7: Find the smallest $M_a \in \mathbb{N}_*$ such that

$$\begin{aligned} \hat{\mathcal{L}}_{\mu_n}[T](\Omega^{(j)}) - \hat{\mathcal{L}}_{\mu_n}[T](R_{\Omega^{(j)}}(\bar{\alpha}\beta^{M_a}\Upsilon^{(j)})) \\ \geq -\sigma_A \langle \nabla \hat{\mathcal{L}}_{\mu_n}[T](\Omega^{(j)}) \mid \bar{\alpha}\beta^{M_a}\Upsilon^{(j)} \rangle_{\Omega^{(j)}} \\ = \sigma_A \bar{\alpha}\beta^{M_a} \|\nabla \hat{\mathcal{L}}_{\mu_n}[T](\Omega^{(j)})\|_{\Omega^{(j)}}^2. \end{aligned}$$

- 8: Define the step-size $t_j^A := \bar{\alpha}\beta^{M_a}$.
- 9: Update $\Omega^{(j+1)} := R_{\Omega^{(j)}}(t_j^A \Upsilon^{(j)})$ via (19).
- 10: **end for**
- 11: $\Omega_n := \Omega^{(J)}$.

detailed in Algorithm 2 and invoked in line 4 of the policy-evaluation step in the PI Algorithm 1—see also Figure 3. To apply Algorithm 2, the gradients in line 5 of the same algorithm must be evaluated, and their closed-form expressions are provided in the following Proposition 7. To avoid also unnecessary clutter in notations, the superscript (n) on the generated data is often omitted.

Proposition 7 (Computing gradients). Consider the estimate $\Omega^{(j)} \in \mathfrak{M}_K$ in line 4 of Algorithm 2, and its associated GMM-QF

$$Q^{(j)}(\cdot) := \sum_{k=1}^K \xi_k^{(j)} \mathcal{G}(\cdot \mid \mathbf{m}_k^{(j)}, \mathbf{C}_k^{(j)}).$$

Let also

$$\begin{aligned} \delta_t^{(j)} &:= g_t + \alpha Q^{(j)}(\mathbf{z}_t') - Q^{(j)}(\mathbf{z}_t), \\ \mathbf{d}_{tk}^{(j)} &:= \alpha \mathcal{G}(\mathbf{z}_t' \mid \mathbf{m}_k^{(j)}, \mathbf{C}_k^{(j)}) \cdot (\mathbf{z}_t' - \mathbf{m}_k^{(j)}) \end{aligned}$$

$$\begin{aligned}
& -\mathcal{G}(\mathbf{z}_t \mid \mathbf{m}_k^{(j)}, \mathbf{C}_k^{(j)}) \cdot (\mathbf{z}_t - \mathbf{m}_k^{(j)}), \\
\bar{\mathbf{d}}_k^{(j)} & := \frac{1}{T} \sum_{t=1}^T \delta_t^{(j)} \mathbf{d}_{tk}^{(j)}, \\
\mathbf{B}_{tk}^{(j)} & := \alpha \mathcal{G}(\mathbf{z}'_t \mid \mathbf{m}_k^{(j)}, \mathbf{C}_k^{(j)}) \cdot (\mathbf{z}'_t - \mathbf{m}_k^{(j)})(\mathbf{z}'_t - \mathbf{m}_k^{(j)})^\top \\
& \quad - \mathcal{G}(\mathbf{z}_t \mid \mathbf{m}_k^{(j)}, \mathbf{C}_k^{(j)}) \cdot (\mathbf{z}_t - \mathbf{m}_k^{(j)})(\mathbf{z}_t - \mathbf{m}_k^{(j)})^\top, \\
\bar{\mathbf{B}}_k^{(j)} & := \frac{1}{T} \sum_{t=1}^T \delta_t^{(j)} \mathbf{B}_{tk}^{(j)}.
\end{aligned}$$

(i) Notice first that the loss in (13) can be recast as $\hat{\mathcal{L}}_\mu[T](\Omega^{(j)}) = (1/T) \|\mathbf{g} + \Delta \boldsymbol{\xi}^{(j)}\|^2$, where $\mathbf{g} := [g_1, \dots, g_T]^\top$ and $\Delta^{(j)}$ is the $T \times K$ matrix having its (t, k) th entry as

$$[\Delta^{(j)}]_{tk} := \alpha \mathcal{G}(\mathbf{z}'_t \mid \mathbf{m}_k^{(j)}, \mathbf{C}_k^{(j)}) - \mathcal{G}(\mathbf{z}_t \mid \mathbf{m}_k^{(j)}, \mathbf{C}_k^{(j)}).$$

Then,

$$\frac{\partial \hat{\mathcal{L}}_\mu[T]}{\partial \boldsymbol{\xi}}(\Omega^{(j)}) = \frac{2}{T} \Delta^{(j)\top} (\mathbf{g} + \Delta^{(j)} \boldsymbol{\xi}^{(j)}). \quad (18a)$$

(ii) $\forall k \in \overline{1, K}$,

$$\frac{\partial \hat{\mathcal{L}}_\mu[T]}{\partial \mathbf{m}_k}(\Omega^{(j)}) = 4 \xi_k^{(j)} (\mathbf{C}_k^{(j)})^{-1} \bar{\mathbf{d}}_k^{(j)}. \quad (18b)$$

(iii) Under the Affl metric and $\forall k \in \overline{1, K}$,

$$\frac{\partial \hat{\mathcal{L}}_\mu[T]}{\partial \mathbf{C}_k}(\Omega^{(j)}) = 2 \xi_k^{(j)} \bar{\mathbf{B}}_k^{(j)} \in \mathbb{S}^{D_z}. \quad (18c)$$

On the other hand, under the BW metric,

$$\begin{aligned}
& \frac{\partial \hat{\mathcal{L}}_\mu[T]}{\partial \mathbf{C}_k}(\Omega^{(j)}) \\
& = 4 \xi_k^{(j)} [(\mathbf{C}_k^{(j)})^{-1} \bar{\mathbf{B}}_k^{(j)} + \bar{\mathbf{B}}_k^{(j)} (\mathbf{C}_k^{(j)})^{-1}] \in \mathbb{S}^{D_z}.
\end{aligned} \quad (18d)$$

Proof. See Appendix D. \square

Owing to the Cartesian structure of \mathfrak{M}_K , it is straightforward to verify that the retraction mapping on \mathfrak{M}_K becomes $R_{\Omega}(\cdot) = (R_{\boldsymbol{\xi}}(\cdot), \dots, R_{\mathbf{m}_k}(\cdot), \dots, R_{\mathbf{C}_k}(\cdot), \dots)$. More specifically, within the context of Algorithm 2, and motivated by Examples 5 and 6,

$$R_{\Omega^{(j)}}(t_j^A \boldsymbol{\Upsilon}^{(j)}) = \left(R_{\boldsymbol{\xi}^{(j)}}(t_j^A \boldsymbol{\theta}^{(j)}), \dots, R_{\mathbf{m}_k^{(j)}}(t_j^A \boldsymbol{\mu}_k^{(j)}), \dots, R_{\mathbf{C}_k^{(j)}}(t_j^A \boldsymbol{\Gamma}_k^{(j)}), \dots \right), \quad (19a)$$

$$R_{\boldsymbol{\xi}^{(j)}}(t_j^A \boldsymbol{\theta}^{(j)}) := \boldsymbol{\xi}^{(j)} + t_j^A \boldsymbol{\theta}^{(j)}, \quad (19b)$$

$$R_{\mathbf{m}_k^{(j)}}(t_j^A \boldsymbol{\mu}_k^{(j)}) := \mathbf{m}_k^{(j)} + t_j^A \boldsymbol{\mu}_k^{(j)}, \quad (19c)$$

$$R_{\mathbf{C}_k^{(j)}}(t_j^A \boldsymbol{\Gamma}_k^{(j)}) := \exp_{\mathbf{C}_k^{(j)}}(t_j^A \boldsymbol{\Gamma}_k^{(j)}), \quad (19d)$$

where $\exp_{\mathbf{C}_k^{(j)}}(\cdot)$ stands for any choice of the exponential map on $\mathbb{S}_{++}^{D_z}$; see, for example, (16).

Theorem 8. Let $(\Omega^{(j)})_{j \in \mathbb{N}_*}$ be the sequence of estimates generated by Algorithm 2. Then, every accumulation point Ω_* of $(\Omega^{(j)})_{j \in \mathbb{N}_*}$ is a critical point of the loss, i.e., $\nabla \hat{\mathcal{L}}_{\mu_n}[T](\Omega_*) = \mathbf{0}$.

Proof. See [30, §4.3.3]. \square

It is worth adding to Theorem 8 that, due to the non-convexity of the objective $\hat{\mathcal{L}}_{\mu_n}[T]$, locating its critical points

does not guarantee the identification of its global minimizers. Nevertheless, the Armijo condition [30, 45] in line 7 of Algorithm 2, used as a backtracking strategy, guarantees a sufficient decrease of the loss [45, Cor. 4.13, p. 63]. Moreover, rather than letting $j \rightarrow \infty$ to locate a critical point as suggested by Theorem 8, Algorithm 2 adopts a more pragmatic approach by introducing a finite iteration budget J , effectively implementing an ‘‘early-stopping’’ strategy similar to that commonly used in neural-network training to mitigate overfitting [46].

C. Performance analysis of Algorithm 1

For the following discussion, a probability space $(\Lambda, \mathfrak{F}, \mathbb{P})$ is considered, where Λ is the sample space, with $\lambda \in \Lambda$, \mathfrak{F} is the σ -algebra of the events on Λ , and \mathbb{P} denotes a probability measure on \mathfrak{F} [40–42]. State vectors \mathbf{s} and action vectors \mathbf{a} will henceforth be regarded as observations (realizations) of the random variables (RVs) s and \mathbf{a} on $(\Lambda, \mathfrak{F}, \mathbb{P})$, respectively. Likewise, the slanted z will be used to denote the ‘‘state-action’’ RV whose observation is $\mathbf{z} = \zeta(\mathbf{s}, \mathbf{a})$.

To sidestep unnecessary technical complications, it is assumed that all RVs admit a probability density function (PDF) [40, §6.12]—for example, the PDF of the RV z is denoted by $p_z(\cdot): \mathfrak{Z} \rightarrow [0, +\infty]: \mathbf{z} \mapsto p_z(\mathbf{z})$. As such, $\mathbb{E}\{|Q(z)|^2\} := \int_{\Lambda} |Q(z(\lambda))|^2 \mathbb{P}(d\lambda) = \int_{\mathfrak{Z}} |Q(z)|^2 p_z(z) dz$ [40, §6.12], where $\mathbb{E}\{\cdot\}$ stands for expectation, defined as the integral w.r.t. \mathbb{P} . Recall also the well-known Hilbert space $L_2(\mathbb{P}) := L_2(\Lambda, \mathfrak{F}, \mathbb{P}) := \{Q(z) \mid \mathbb{E}\{|Q(z)|^2\} < +\infty\}$, endowed with the inner product $\langle Q(z) \mid Q'(z') \rangle_{L_2(\mathbb{P})} := \mathbb{E}\{Q(z)Q'(z')\}$ [40].

Lemma 9. The RV $Q(z) \in L_2(\Lambda, \mathfrak{F}, \mathbb{P})$ if and only if the Q-function $Q \in L_2(\mathfrak{P}_z) := L_2(\mathfrak{Z}, \mathfrak{B}(\mathfrak{Z}), \mathfrak{P}_z)$, where $\mathfrak{B}(\mathfrak{Z})$ stands for the Borel σ -algebra on \mathfrak{Z} , and the Borel probability measure \mathfrak{P}_z is induced by the PDF $p_z(\cdot)$ as $\mathfrak{P}_z(\mathcal{B}) := \int_{\mathcal{B}} p_z(z) dz$, $\forall \mathcal{B} \in \mathfrak{B}(\mathfrak{Z})$.

Proof. The proof follows verbatim the proof of the lemma in [40, §6.12]. \square

Assumptions 10.

- (i) Any two state-action RVs z, z' are identically distributed, that is, $p_z(\cdot) = p_{z'}(\cdot)$, almost everywhere (a.e.) on \mathfrak{Z} . Consequently, the induced measure \mathfrak{P}_z in Lemma 9 remains invariant w.r.t. the choice of the RV z and will be denoted hereafter by \mathfrak{P} .
- (ii) The one-step loss $g(\cdot)$ belongs to $L_2(\mathfrak{P})$.

Owing to Assumption 10(i), Lemma 9 now provides the direct connection between the present discussion and Theorem 3(ii). In particular, under Assumption 2 and Assumption 10(i), Theorem 3(ii) shows that $\cup_{K \in \mathbb{N}_*} \mathcal{Q}_K$ is dense in $L_2(\mathfrak{Z}, \mathfrak{B}(\mathfrak{Z}), \mathfrak{P})$. Assumption 10(ii) is used in Proposition 11 to demonstrate that the classical Bellman mappings \mathcal{T}_μ^\diamond and \mathcal{T}^\diamond are well defined on $L_2(\mathfrak{P})$.

Proposition 11. Under Assumptions 10(i) and 10(ii), the Bellman mappings $\mathcal{T}_\mu^\diamond, \mathcal{T}^\diamond$ in (1) map the Hilbert space $L_2(\mathfrak{P})$ into itself. More specifically, they are contractions [35]—that is, $\forall Q_1, Q_2 \in L_2(\mathfrak{P}), \forall \mu \in \mathcal{M}$, and regardless of the choice of the state-action RV z ,

$$\|\mathcal{T}_\mu^\diamond Q_1 - \mathcal{T}_\mu^\diamond Q_2\|_{L_2(\mathfrak{P})}$$

$$\begin{aligned}
&= \left(\mathbb{E} \{ |(\mathcal{T}_\mu^\diamond Q_1)(z) - (\mathcal{T}_\mu^\diamond Q_2)(z)|^2 \} \right)^{\frac{1}{2}} \\
&\leq \alpha \left(\mathbb{E} \{ |Q_1(z) - Q_2(z)|^2 \} \right)^{\frac{1}{2}} = \alpha \|Q_1 - Q_2\|_{L_2(\mathfrak{F})}, \\
&\|\mathcal{T}^\diamond Q_1 - \mathcal{T}^\diamond Q_2\|_{L_2(\mathfrak{F})} \\
&= \left(\mathbb{E} \{ |(\mathcal{T}^\diamond Q_1)(z) - (\mathcal{T}^\diamond Q_2)(z)|^2 \} \right)^{\frac{1}{2}} \\
&\leq \alpha \left(\mathbb{E} \{ |Q_1(z) - Q_2(z)|^2 \} \right)^{\frac{1}{2}} = \alpha \|Q_1 - Q_2\|_{L_2(\mathfrak{F})},
\end{aligned} \tag{20a}$$

where the discount factor $\alpha \in [0, 1)$.

Proof. See Appendix E. \square

Because \mathcal{T}_μ^\diamond and \mathcal{T}^\diamond are contractions in the Hilbert space $L_2(\mathfrak{F})$, they each have a unique fixed point, denoted Q_μ^\diamond and Q^\diamond , respectively [35]. The classical method to compute these fixed points is the Banach-Picard iteration: for any arbitrarily fixed $Q \in L_2(\mathfrak{F})$, sequences $((\mathcal{T}_\mu^\diamond)^i Q)_{i \in \mathbb{N}_*}$ and $((\mathcal{T}^\diamond)^i Q)_{i \in \mathbb{N}_*}$ converge to Q_μ^\diamond and Q^\diamond , respectively, as $i \rightarrow \infty$ [35].

If data $\{(\mathbf{z}_t, \mathbf{z}'_t)\}_{t=1}^T$ are assumed to be observations (realizations) of the independent and identically distributed (IID) RVs $\{(\mathbf{z}_t = \zeta(\mathbf{s}_t, \mathbf{a}_t), \mathbf{z}'_t = \zeta(\mathbf{s}'_t, \mu(\mathbf{s}'_t)))\}_{t=1}^T$, for some stationary policy μ , a strong connection between the empirical loss $\hat{\mathcal{L}}_\mu[T](\cdot)$ in (5) and the ensemble $\mathcal{L}_\mu(\cdot)$ one in (6) emerges. This is because, according to the strong law of large numbers [41, §6.2.5], $\forall Q \in L_2(\mathfrak{F})$,

$$\begin{aligned}
\hat{\mathcal{L}}_\mu[T](Q) &= \frac{1}{T} \sum_{t=1}^T [g(\mathbf{z}_t) + \alpha Q(\mathbf{z}'_t) - Q(\mathbf{z}_t)]^2 \\
&\xrightarrow[T \rightarrow \infty]{\text{a.s.}} \mathbb{E} \{ [g(\mathbf{z}) + \alpha Q(\mathbf{z}') - Q(\mathbf{z})]^2 \} =: \mathcal{L}_\mu(Q),
\end{aligned} \tag{21}$$

where convergence holds almost surely (a.s.).

The following lemma provides an equivalent formulation of the ensemble loss, thereby aiding the subsequent analysis.

Lemma 12. For any $Q \in L_2(\mathfrak{F})$ and any stationary policy μ ,

$$\begin{aligned}
\mathcal{L}_\mu(Q) &= \alpha^2 \mathbb{E} \{ \mathbb{V}_{\mathbf{s}'|\mathbf{z}} \{ Q(\zeta(\mathbf{s}', \mu(\mathbf{s}')))) \} \} \\
&\quad + \|Q - \mathcal{T}_\mu^\diamond Q\|_{L_2(\mathfrak{F})}^2,
\end{aligned}$$

where the conditional variance

$$\mathbb{V}_{\mathbf{s}'|\mathbf{z}} \{ Q(\mathbf{z}') \} := \mathbb{E}_{\mathbf{s}'|\mathbf{z}} \{ [Q(\mathbf{z}') - \mathbb{E}_{\mathbf{s}'|\mathbf{z}} \{ Q(\mathbf{z}') \}]^2 \},$$

with $\mathbf{z}' = \zeta(\mathbf{s}', \mu(\mathbf{s}'))$.

Proof. See Appendix F. \square

Lemma 12 indicates that a minimizer of the ensemble BR loss $\mathcal{L}_\mu(\cdot)$ does not coincide in general with the unique fixed point Q_μ^\diamond of \mathcal{T}_μ^\diamond —recall that $Q_\mu^\diamond = \mathcal{T}_\mu^\diamond Q_\mu^\diamond$. In other words, minimizing the empirical loss $\hat{\mathcal{L}}_\mu[T]$, which lies close to \mathcal{L}_μ for large values of the number T of data samples according to (21), often yields a biased estimate of Q_μ^\diamond . This issue is well known in BR schemes and is typically addressed either through the introduction of auxiliary functions [10, 47] or by employing double sampling techniques [2, 13, 15].

Motivated by the previous discussion, the following assumptions are introduced.

Assumptions 13.

(i) There exist a sufficiently large number $T_{\mathcal{E}_\#} \in \mathbb{N}_*$ and a $\delta_{\mathcal{E}_\#} \in \mathbb{R}_{++}$ s.t. for any number $T \geq T_{\mathcal{E}_\#}$ of samples and any stationary policy μ , data $\{(\mathbf{z}_t, \mathbf{z}'_t)\}_{t=1}^T$ are evaluations (realizations) of the RVs $\{(\mathbf{z}_t = \zeta(\mathbf{s}_t, \mathbf{a}_t), \mathbf{z}'_t = \zeta(\mathbf{s}'_t, \mu(\mathbf{s}'_t)))\}_{t=1}^T$ at a sample point taken from the following nonempty event of the probability space:

$$\mathcal{E}_\# := \left\{ \lambda \in \Lambda \mid \sup_{\substack{Q \in C(3), \\ \mu \in \mathcal{M}}} |\mathcal{L}_\mu(Q) - \hat{\mathcal{L}}_\mu[T](Q)| \leq \delta_{\mathcal{E}_\#} \right\}.$$

(ii) For any observed data, there exists a $\Delta \in \mathbb{R}_{++}$ s.t. the outcome of Algorithm 2 yields, $\forall n \in \mathbb{N}$ and a.s.,

$$\hat{\mathcal{L}}_{\mu_n}[T](Q_n) \leq \inf_{Q \in \mathcal{Q}_K} \hat{\mathcal{L}}_{\mu_n}[T](Q) + \Delta.$$

(iii) There exists a $\delta_{\text{inf}} \in \mathbb{R}_{++}$ s.t. for sufficiently large K , for any stationary policy μ and a.s.,

$$\inf_{Q \in \mathcal{Q}_K} \hat{\mathcal{L}}_\mu[T](Q) \leq \inf_{Q \in \cup_{K' \in \mathbb{N}_*} \mathcal{Q}_{K'}} \hat{\mathcal{L}}_\mu[T](Q) + \delta_{\text{inf}}.$$

(iv) (**Bounded expected conditional variance**) There exists $\sigma_V \in \mathbb{R}_{++}$ and a sufficiently small $\delta_\diamond \in \mathbb{R}_{++}$ s.t. $\forall n \in \mathbb{N}$,

$$\sup_{\tilde{Q} \in B[\mathcal{Q}_{\mu_n}^\diamond, \delta_\diamond]} \mathbb{E} \{ \mathbb{V}_{\mathbf{s}'|\mathbf{z}} \{ \tilde{Q}(\zeta(\mathbf{s}', \mu_n(\mathbf{s}')))) \} \} \leq \sigma_V^2,$$

where the ball $B[\mathcal{Q}_{\mu_n}^\diamond, \delta_\diamond] := \{Q \in L_2(\mathfrak{F}) \mid \|Q - \mathcal{Q}_{\mu_n}^\diamond\|_{L_2(\mathfrak{F})} \leq \delta_\diamond\}$.

(v) There exists $\Delta_2 \in \mathbb{R}_{++}$ s.t. for all sufficiently large n ,

$$\|\mathcal{Q}_{\mu_{n+1}}^\diamond - \mathcal{Q}_{\mu_n}^\diamond\|_{L_2(\mathfrak{F})} \leq \Delta_2.$$

Assumption 13(i) is motivated by (21). The IID assumption underlying (21) is common in statistical performance analyses beyond RL. In contrast, Assumption 13(i) relaxes the IID requirement by imposing only a boundedness condition, while simultaneously introducing a uniformity constraint that is typically absent from standard IID settings. Assumption 13(ii) reflects the expectation that Algorithm 2 produces an estimate that remains, up to some Δ , above the infimum of the empirical BR loss. Although first-order schemes like Algorithm 2 do not guarantee convergence to a global minimizer, the Armijo line search ensures sufficient decrease at each iteration, driving the iterates into a neighborhood of a critical point—see Theorem 8. Assumption 13(iii) follows the same spirit. It assumes that the user chooses K large enough so that minimization over the approximation space \mathcal{Q}_K is within δ_{inf} of the infimum over the full union $\cup_{K' \in \mathbb{N}_*} \mathcal{Q}_{K'}$ —notice that $\mathcal{Q}_k \subset \mathcal{Q}_{k+1}$, $\forall k$. Assumption 13(iv) is motivated by [48], which studies a simpler RL setting in “mildly stochastic” environments, especially in offline RL, where simulated data are used for training. Finally, Assumption 13(v) is motivated by a related discussion in [15] and imposes a smoothness condition on the fixed points $(\mathcal{Q}_{\mu_n}^\diamond)_n$ for all sufficiently large n .

Proposition 14.

(i) Under Assumption 2 and Assumptions 13(i) to 13(iv),

$$\limsup_{n \rightarrow \infty} \|Q_n - \mathcal{Q}_{\mu_n}^\diamond\|_{L_2(\mathfrak{F})} \leq \underbrace{\frac{\sqrt{\alpha^2 \sigma_V^2 + \delta_{\text{inf}} + \Delta + 2\delta_{\mathcal{E}_\#}}}{1 - \alpha}}_{\Delta_1}.$$

(ii) Under Assumption 2 and Assumptions 13,

$$\limsup_{n \rightarrow \infty} \|Q_n - Q^\diamond\|_{L_2(\mathfrak{F})} \leq \Delta_1 + \frac{\alpha}{1-\alpha}(2\Delta_1 + \Delta_2),$$

where Q^\diamond is the unique fixed point of \mathcal{T}^\diamond —see Proposition 11.

Proof. See Appendix G. \square

A result similar to the one in Proposition 14(i) appears as an assumption in [1, (5.11)], which is used in the proof of [1, Prop. 5.1.4] to establish convergence of approximate policy iteration. However, the analysis in [1, Prop. 5.1.4] is conducted in the context of $\|\cdot\|_\infty$, whereas the present discussion is carried out in $L_2(\mathfrak{F})$, with assumptions justified for the $\|\cdot\|_{L_2(\mathfrak{F})}$ norm. To establish Proposition 14(i), Assumption 13(v) is required. Proposition 14(ii) then bounds the distance of the sequence of estimates $(Q_n)_{n \in \mathbb{N}_*}$ from the fixed point Q^\diamond , thereby establishing the stability and consistency of Algorithm 1 with respect to the classical Bellman mapping \mathcal{T}^\diamond .

D. Computational complexity of Algorithm 1

The computational cost of Algorithm 1 at each policy iteration n is governed by the complexity of Algorithm 2. Per iteration j , the dominant cost arises from computing Riemannian gradients and performing retractions on \mathfrak{M}_K . In particular, $\partial \mathcal{L}_{\mu_n}[T](\cdot)/\partial \xi$ in (18a) requires $\mathcal{O}(TK)$ operations due to averaging over T samples, where $\mathcal{O}(\cdot)$ denotes the big-O (Bachmann-Landau) notation [49]. For each Gaussian component $\mathcal{G}_k(\cdot)$, $\partial \mathcal{L}_{\mu_n}[T](\cdot)/\partial \mathbf{m}_k$ in (18b) and $\partial \mathcal{L}_{\mu_n}[T](\cdot)/\partial \mathbf{C}_k$ in (18c) and (18d) incur a cost of $\mathcal{O}(TK(D_z + D_z(D_z + 1)/2)) = \mathcal{O}(TKD_z^2)$. The inversion of $\{\mathbf{C}_k\}_{k=1}^K \subset \mathbb{S}_{++}^{D_z}$ scales on the order of $\mathcal{O}(KD_z^3)$. Consequently, the total complexity of gradient computation is $\mathcal{O}(KD_z^2(D_z + T))$.

Retractions for $\xi \in \mathbb{R}^K$ and $\mathbf{m}_k \in \mathbb{R}^{D_z}$ in Euclidean spaces are simple with cost $\mathcal{O}(K(1 + D_z))$. On the other hand, retractions the manifold $\mathbb{S}_{++}^{D_z}$ in (16) require either computing a matrix exponential (Affl metric) or solving a Lyapunov equation (BW metric), each with complexity of $\mathcal{O}(D_z^3)$ per Gaussian component. Since line 7 in Algorithm 2 may require M_a iterations to identify the Armijo step-size, the overall computational complexity associated with retractions is $\mathcal{O}(KM_a(1 + D_z + D_z(D_z + 1)/2) + KD_z^3) = \mathcal{O}(KD_z^2(D_z + M_a))$. Combining the above terms, running Algorithm 2 with J iterations incurs an overall computational complexity of $\mathcal{O}(JKD_z^2(M_a + D_z + T))$. Although M_a may be unbounded, in practice the total cost can always be reduced by imposing an upper limit on the line-search depth in Algorithm 2. On the other hand, the computational complexity of GMM-QFs via Riemannian optimization also increases with the number of Gaussian components. A practical remedy is to update only a randomly selected subset of gradient entries per iteration n —an approach closely related to feature-selection strategies for GMM-QFs and one that will be explored in future studies.

Computational complexity of deep RLs is primarily determined by the underlying DNN architecture. For a network with layer sizes $[h_0, h_1, \dots, h_L]$, with $h_0 := D_s$, $h_L := |\mathfrak{A}|$, the cost, which scales also with the number of samples

T , is $\mathcal{O}(T \sum_{l=1}^L h_{l-1} h_l)$. In practice, capturing task-specific nonlinearities often requires deep and wide networks, leading to significantly computational overhead.

In contrast, nonparametric methods, such as KBRL and distributional RL, typically incur lower computational complexity at early stages of learning. However, their complexity is dominated by the size of their approximation basis, which grows upon the arrival of new data. For example, distributional RL methods that utilize GMMs via EM require a per-iteration computational cost of $\mathcal{O}(K_{\text{dist}} D_z^3)$, with K_{dist} being the size of the current basis. A detailed analysis of computational complexity of KBRL can be found in [15].

V. NUMERICAL TESTS

Three classical benchmark RL tasks, the *inverted pendulum* [50], the *mountain car* [51] and the *acrobot* [52] are selected to validate the proposed Algorithm 1 against:

- (i) Kernel-based least-squares policy iteration (KLSPI) [11], which utilizes LSTD in an RKHS;
- (ii) online Bellman residual (OBR) [12];
- (iii) the popular deep Q-network (DQN) [18];
- (iv) the dueling double (D)DQN [53], which, similarly to DQN, uses deep neural networks and experience data to train the Q-functions;
- (v) the proximal policy optimization (PPO) [54], a representative of policy-based methods; and
- (vi) the GMM-based RL [24] via an online EM algorithm (EM-GMMRL).

To validate performance, the coordinate of the vertical axis in Figures 5 to 9 measures the total number of steps the agent needs to take to reach the “goal” of the task, starting from a pre-defined “resting position” and operating under policy μ_n . The coordinate n of the horizontal axis in Figures 5 to 8, called also “number of trials” here, is the iteration index of the PI Algorithm 1. In other words, the closer a curve lies to the bottom-left corner of the figure, the higher the learning efficiency of the RL algorithm that produces it. All results are averaged over multiple independent runs. The software was implemented in Julia [55] and Python.

A. Inverted pendulum

This environment concerns the task of swinging a pendulum from its lowest position to the upright one using a limited set of available torques [50]. The optimal policy is nontrivial to obtain because, given the torque constraints and the effect of gravity, the controller must swing the pendulum back and forth until sufficient kinetic energy is accumulated to reach the desired upright position (Figure 4a).

The state $\mathbf{s} := [\theta, \dot{\theta}]^\top$, where $\theta \in [-\pi, \pi]$ is the angular position ($\theta = 0$ corresponds to the upright position), and $\dot{\theta} \in [-4, 4]s^{-1}$ is the angular velocity. The action space is the set of torques $\mathfrak{A} := \{-5, -3, 0, 3, 5\}N$. The one-step loss is defined as $g(\zeta(\mathbf{s}, \mathbf{a})) := 0$, if $\theta = 0$, and $g(\zeta(\mathbf{s}, \mathbf{a})) := 1$, if $\theta \neq 0$.

To collect data samples $\mathcal{D}_{\mu_n}[T]$ in Algorithm 1, the pendulum starts from an angular position and explores a number of actions under the current policy μ_n . This exploration is called an episode, and per iteration n in Algorithm 1, data $\mathcal{D}_{\mu_n}[T]$

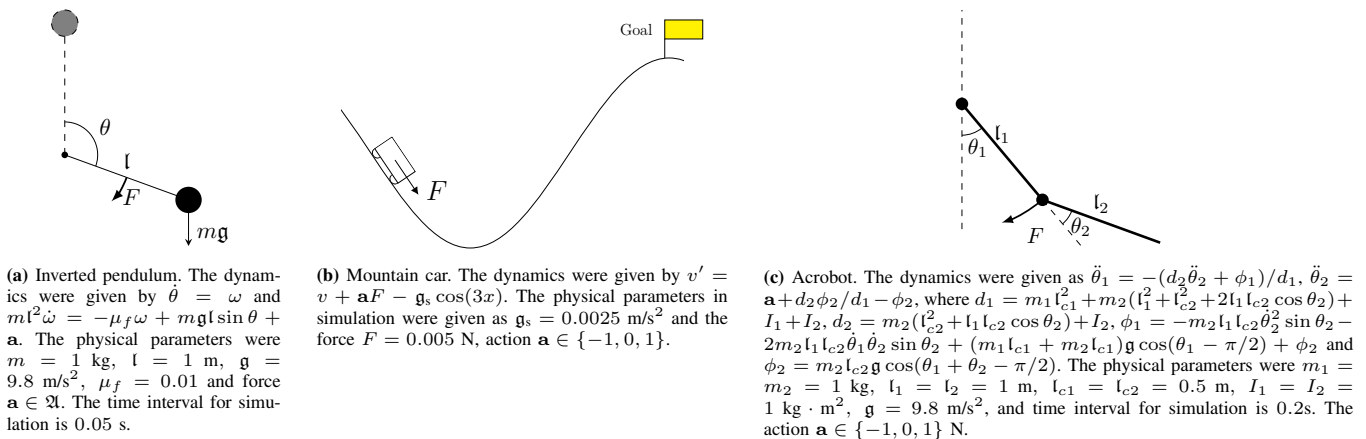


Fig. 4: Control tasks considered in Section V. The dynamics of the systems given above are only used for simulation.

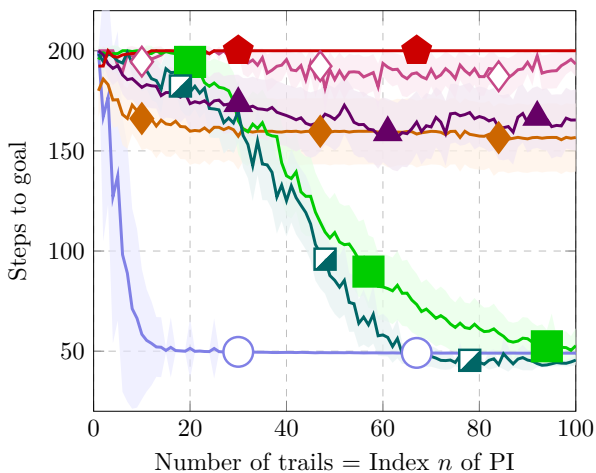


Fig. 5: Inverted-pendulum dataset. Curve markers: Algorithm 1 (AffInv) with $K = 5$: \circ , KLSPI [11]: \diamond , OBR [12]: \diamond , DQN [18]: \square , Dueling DDQN [53]: \square , PPO [54]: \triangle , EM-GMMRL [24]: \diamond .

with $T := (\text{number of episodes}) \times (\text{number of actions}) = 20 \times 70 = 1400$ are collected. KLSPI [11] and OBR [12] use the Gaussian kernel with bandwidth $\sigma_\kappa = 2$, while their ALD threshold is $\delta_{\text{ALD}} = 0.01$. KLSPI and OBR need $T = 5000$ to reach their “optimal” performance for the task at hand. DQN [18] and dueling DDQN [53] use a fully-connected neural network for Q-functions with 2 hidden layers of size 128, with batch size of 64, and a replay buffer (experience data) of size 1×10^5 , while PPO [54] uses an additional neural network with the same configuration for the policy. For EM-GMMRL [24], $T = 500$, while its threshold to add new Gaussian functions in its dictionary is 10^{-4} . For Algorithm 1 and EM-GMMRL is defined as $\zeta(\mathbf{s}, \mathbf{a}) := (\mathbf{s}, \mathbf{a} / \max_{\mathbf{a} \in \mathfrak{A}} |\mathbf{a}|)$; while $\zeta(\mathbf{s}, \mathbf{a})$ in KLSPI and OBR is defined via a Kronecker product, following the setting of [56].

As shown in Figure 5, the proposed Algorithm 1 achieves the best performance without using a replay buffer (experience data), in contrast to DQN [18] and dueling DDQN [53], which require large replay buffers and exhibit slower learning and higher variance than GMM-QFs. PPO [54] underperforms within the first 100 iterations. It is well known that PPO, as well as other policy-based methods, converges more slowly

and requires more data than value-based approaches. KLSPI [11] attains suboptimal performance, while OBR [12] and EM-GMMRL [24] fail to achieve satisfactory results. Notably, KLSPI and OBR are provided with more exploration data than Algorithm 1. Finally, EM algorithms are known to be sensitive to initialization [29], a fact that was also verified in the present tests through the use of several initialization strategies.

B. Mountain car

This setting describes a car placed at the bottom of a sinusoidal valley, where the slope is given by $y = \sin(3x)$ in the xy -plane, with $x \in [-1.2, 0.6]$ [51]. The only available actions are accelerations applied to the car in either direction. The objective is to strategically accelerate the car, using both directions, to accumulate sufficient kinetic energy to reach the terminal (goal) state at the top of the hill (Figure 4b).

The state $\mathbf{s} := [x, v]^T$, where the velocity of the car $v \in [-0.07, 0.07]$. The goal is achieved when the car gets beyond $x_g := 0.5$ with velocity larger than or equal to $v_g := 0$, that is, whenever the car reaches a state in $\mathfrak{S}_g := \{[x, v]^T \mid x \geq x_g, v \geq v_g\}$. The one-step loss is defined as $g(\mathbf{s}, \mathbf{a}) := 1$, if $\mathbf{s} \notin \mathfrak{S}_g$, while $g(\zeta(\mathbf{s}, \mathbf{a})) := 0$, if $\mathbf{s} \in \mathfrak{S}_g$. The state-action $\zeta(\mathbf{s}, \mathbf{a})$ is defined similarly to Section V-A.

With regards to the data $\mathcal{D}_{\mu_n}[T]$ in Algorithm 1, a strategy similar to that of the inverted pendulum is used. More specifically, $T = 1000$ for the proposed GMM-QFs, while $T = 20000$ for KLSPI [11] and $T = 1000$ for OBR [12]. A Gaussian kernel with width of $\sigma_\kappa = 0.1$ is used for KLSPI [11] and OBR [12]. The implementation of DQN [18], dueling DDQN [53], PPO [54] is identical to ones for the inverted-pendulum case, while exploration length is set as $T = 100$ for EM-GMMRL [24].

Due to the fluctuation in performance of all algorithms, moving average values on the curves, with window size of 10, are employed hereafter.

In Figure 6, DQN [18] achieves the best performance, followed by PPO [54] and GMM-QFs with $K = 500$. Note that DQN relies on a large amount of experience data (with a replay buffer of size 1×10^5), whereas the proposed GMM-QFs require *no* experience data to attain the performance

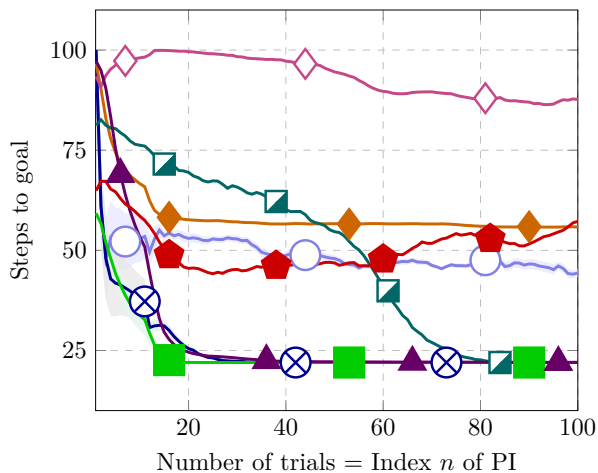


Fig. 6: Mountain-car dataset. Curve markers: GMM-QFs (Affl) with $K = 500$: \otimes , others follow Figure 5.

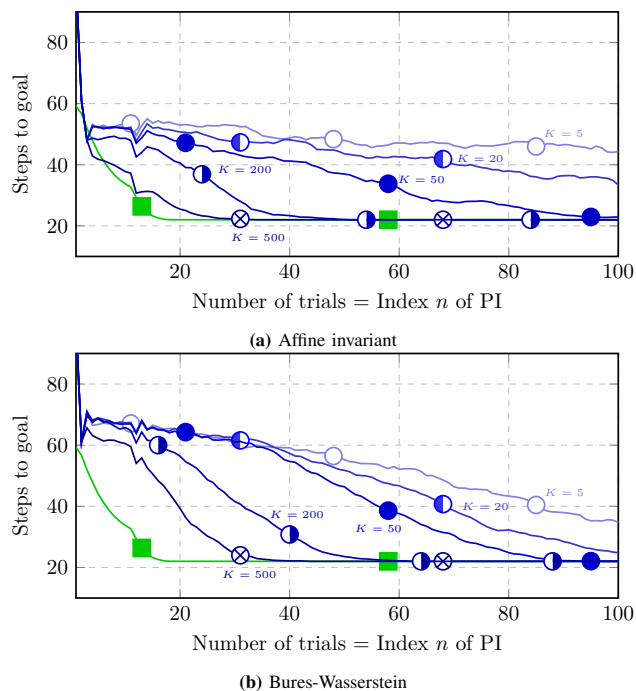


Fig. 7: Effect of different K in Algorithm 1 for the setting of mountain car. Curve markers (for both Affl and BW) $K = 20$: \circ , $K = 50$: \bullet , $K = 200$: \circ , DQN [18]: \blacksquare as a baseline. The larger the K , the richer the hyperparameter space \mathfrak{M}_K becomes and the faster the agent learns through the feedback from the environment, at the expense of increased computational complexity.

shown in Figure 6. It can also be observed that increasing the number K of Gaussian components in (7) allows GMM-QFs to reach the optimal performance of DQN in Figure 6, albeit at the cost of increased computational complexity; see also Figure 7. OBR [12] and EM-GMMRL [23] perform better in this setting than in the inverted pendulum task, with EM-GMMRL exhibiting stronger learning behavior than OBR.

C. Acrobot

This setting considers a more challenging control problem. The acrobot, also known as the *double-linked pendulum*, is

a class of underactuated robots widely studied in optimal control [52]. As illustrated in Figure 4c, the acrobot consists of two links connected in a chain, with one end fixed. An actuator is located at the joint and is used to swing the free end of the chain from the initial downward-hanging configuration to the upright position. As in the traditional inverted pendulum, the objective is to reach the desired position in as few steps as possible, without prior knowledge of the system dynamics. Due to its strong nonlinearity and chaotic behavior, the acrobot task is considerably more challenging than the previously considered environments.

The state $\mathbf{s} := [\theta_1, \theta_2, \dot{\theta}_1, \dot{\theta}_2]^\top$, where $\theta_i \in [-\pi, \pi]$ is the angular position, and $\dot{\theta}_i$ is the angular velocity of link i with $i = 1, 2$. The angular velocity is bounded differently between 2 links, as $\dot{\theta}_1 \in [-4\pi, 4\pi]\text{s}^{-1}$ and $\dot{\theta}_2 \in [-9\pi, 9\pi]\text{s}^{-1}$. In this experiment, the goal is achieved when $\mathbf{s} \in \mathfrak{S}_g := \{[\theta_1, \theta_2, \dot{\theta}_1, \dot{\theta}_2]^\top \mid -\cos(\theta_1) - \cos(\theta_1 + \theta_2) > 1\}$. The one-step loss is defined accordingly, as $g(\zeta(\mathbf{s}, \mathbf{a})) := 0$ if $\mathbf{s} \in \mathfrak{S}_g$, and $g(\zeta(\mathbf{s}, \mathbf{a})) := 1$ otherwise.

In contrast to the previous two settings, and along the lines of [9], the GMM-QFs' weight vector ξ is made dependent on the action $\mathbf{a} \in \mathfrak{A}$, so that each action gets its own weights. In particular,

$$Q(\mathbf{s}, \mathbf{a}) := \sum_{k=1}^K \xi_k^{(\mathbf{a})} \mathcal{G}(\mathbf{s} \mid \mathbf{m}_k, \mathbf{C}_k), \quad \forall (\mathbf{s}, \mathbf{a}),$$

with $\mathcal{G}(\cdot \mid \mathbf{m}_k, \mathbf{C}_k)$ defined as in (3). Owing to this new setting for the weight vectors, the Cartesian-product manifold for Algorithm 2 now becomes $\mathfrak{M}_K := (\mathbb{R}^K)^{|\mathfrak{A}|} \times (\mathbb{R}^{D_s})^K \times (\mathbb{S}_{++}^{D_s})^K$, with D_s being the dimension of state \mathbf{s} .

The dataset $\mathcal{D}_{\mu_n}[T]$ is collected by running 20 exploration episodes, each consisting of 70 sequential state transitions. In other words, $T = 20 \times 70 = 1400$ for Algorithm 1. Datasets of the same size are used for OBR [12], DQN [18], dueling DDQN [53], and PPO [54]. For KLSPI [11], a larger dataset of $T = 100$ (episodes) \times 500 (state transitions) is employed. All other configurations for the deep RL methods are identical to those used in the inverted pendulum case, except that the replay buffer size for DQN is set to 10^4 . For EM-GMMRL [24], $T = 1500$ is used, and the threshold for updating its dictionary is set to 1×10^{-6} .

As shown in Figure 8, Algorithm 1 with $K = 50$ and $K = 500$ (Affl metric), together with DQN [18] and PPO [54], outperforms the other methods by reaching a stable regime starting from approximately the 70th trial. The policies learned by OBR [12] and dueling DDQN [53] improve slowly, even when both new and replayed experience data are provided during training. In contrast, KLSPI [11] exhibits suboptimal performance, while EM-GMMRL [24] fails to achieve the desired behavior. It is also noteworthy that GMM-QFs with $K = 500$ slightly underperform those with $K = 50$. This apparent suboptimality can be attributed to the biased nature of the Bellman-residual loss toward the current policy. This clearly raises issues related to model-size selection. Developing strategies for automatically choosing appropriate model sizes for GMM-QFs is left for future work.

Among the successful methods, DQN [18] and PPO [54] both require at least a two-layer fully connected network with

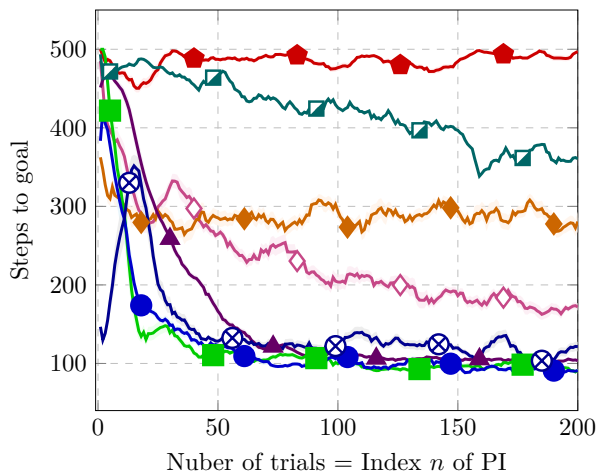


Fig. 8: Acrobot dataset. Curve markers: Algorithm 1 (AffI) with $K = 50$: \bullet , $K = 500$: \otimes , others follow Figure 5. Window size for moving average is set as 10.

128 hidden neurons per layer to achieve the performance reported in Figure 8, resulting in a large number of learnable parameters. In contrast, Algorithm 1 attains comparable performance with significantly fewer parameters, leading to substantially lower computational resource consumption (see Table I). Beyond model size, the computational cost of Algorithm 1 is dominated by policy evaluation, which scales with a fixed iteration budget J . As a result, Algorithm 1 with GMM-QFs is computationally more efficient than deep RL methods. By comparison, the computational burden of DQN and PPO depends primarily on their network architectures. Although this overhead can be reduced by adopting “tiny” configurations, such reductions typically come at the expense of overall performance (see Figure 9). On the other hand, GMM-QFs with a larger number of Gaussian components K generally require a larger evaluation budget J to reach optimal performance, which ultimately increases computational complexity.

TABLE I: Number of learned parameters (acrobot)

Methods	# parameters
Algorithm 1 ($K = 50$)	850 (50 Gaussian functions)
Algorithm 1 ($K = 500$)	8500 (500 Gaussian functions)
DQN [18]	17 795 (2 128-neuron layers)
PPO [54]	35 332 (2 networks, 2 128-neuron layers)

VI. CONCLUSIONS

This paper introduced a novel class of Gaussian-mixture-model Q-functions (GMM-QFs) together with a Riemannian-optimization-based learning framework for estimating their hyperparameters, serving as a new policy-evaluation step within a policy-iteration scheme for reinforcement learning (RL). The proposed GMM-QFs are parametric, possess universal approximation properties, and provide competitive representational capacity compared to conventional deep RL methods, while requiring significantly fewer learnable parameters. This results in improved computational efficiency and alleviates limitations commonly associated with nonparametric approaches.

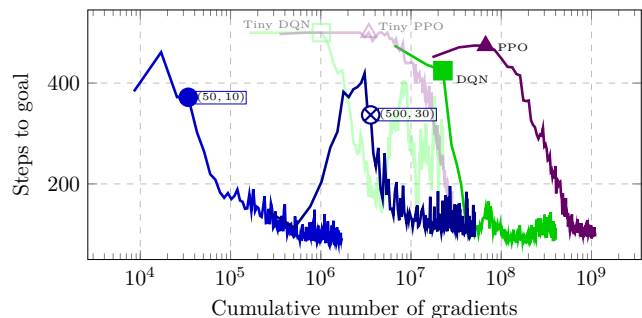


Fig. 9: Performance of Algorithm 1, DQN [18], PPO [54] for acrobot dataset against cumulative number of gradients calculated. Markers: “tiny” DQN [57] (2 hidden layers of 16 neurons): \square , “tiny” PPO (Q-network of 2 16-neuron layers and policy network of 2 8-neuron layers): \triangle . Others follow ones of Figure 8, with annotation on Algorithm 1 indicating both the number of Gaussians K and iteration budget J in form of (K, J) . GMM-QFs with larger K require a larger J , at the cost of increased computational complexity.

The proposed design also offered substantial flexibility, not only through a rich hyperparameter space, but also by establishing a compelling connection between Q-function identification in RL and the powerful toolbox of Riemannian optimization. Numerical tests demonstrated comparable, and often superior, performance relative to state-of-the-art methods, indicating strong potential for extension to practical, particularly online, RL settings.

While the current offline policy-iteration approach based on Bellman residuals may suffer from bias due to the absence of experience data, ongoing work focuses on extending the framework to online RL in high-dimensional environments and on selecting Gaussian components via structured sparsification to enhance interpretability. These extensions are currently under development and will be reported in future publications.

REFERENCES

- [1] D. Bertsekas, *Reinforcement Learning and Optimal Control*. Belmont, MA: Athena Scientific, 2019.
- [2] R. S. Sutton and A. G. Barto, *Reinforcement Learning: An Introduction*. Cambridge, MA: The MIT Press, 2018.
- [3] C. Watkins and P. Dayan, “Q-learning,” *Mach. Learn.*, vol. 8, pp. 279–292, 1992.
- [4] S. Singh, T. Jaakkola, M. L. Littman, and C. Szepesvári, “Convergence results for single-step on-policy reinforcement-learning algorithms,” *Mach. Learn.*, vol. 38, no. 3, pp. 287–308, 2000.
- [5] D. Ormoneit and Š. Sen, “Kernel-based reinforcement learning,” *Mach. Learn.*, vol. 49, pp. 161–178, 2002.
- [6] D. Ormoneit and P. Glynn, “Kernel-based reinforcement learning in average-cost problems,” *IEEE Trans. Auto. Control*, vol. 47, no. 10, pp. 1624–1636, Oct. 2002.
- [7] J. Bae, L. S. Giraldo, P. Chhatbar, J. Francis, J. Sanchez, and J. Príncipe, “Stochastic kernel temporal difference for reinforcement learning,” in *Proc. IEEE Mach. Learn. Signal Process.*, 2011, pp. 1–6. DOI: 10.1109/MLSP.2011.6064634
- [8] R. S. Sutton, “Learning to predict by the methods of temporal differences,” *Mach. Learn.*, vol. 3, no. 1, pp. 9–44, 1988. DOI: 10.1023/A:1022633531479
- [9] M. G. Lagoudakis and R. Parr, “Least-squares policy iteration,” *J. Mach. Learn. Res.*, vol. 4, pp. 1107–1149, Dec. 2003.
- [10] A.-M. Farahmand, M. Ghavamzadeh, C. Szepesvári, and S. Mannor, “Regularized policy iteration with nonparametric function spaces,” *J. Mach. Learn. Res.*, vol. 17, no. 1, pp. 4809–4874, 2016.
- [11] X. Xu, D. Hu, and X. Lu, “Kernel-based least squares policy iteration for reinforcement learning,” *IEEE Trans. Neural Net.*, vol. 18, no. 4, pp. 973–992, 2007. DOI: 10.1109/TNN.2007.899161

- [12] W. Sun and J. A. Bagnell, "Online Bellman residual and temporal difference algorithms with predictive error guarantees," in *Proc. Int. Joint Conf. Art. Intel.*, New York, NY, USA, 2016, pp. 4213–4217.
- [13] M. Vu, Y. Akiyama, and K. Slavakis, "Dynamic selection of p-norm in linear adaptive filtering via online kernel-based reinforcement learning," in *Proc. IEEE Int. Conf. Acoust., Speech, Signal Process.*, Rhodes Island, Greece, 2023, pp. 1–5. DOI: 10.1109/ICASSP49357.2023.10096825
- [14] Y. Akiyama and K. Slavakis, "Proximal Bellman mappings for reinforcement learning and their application to robust adaptive filtering," in *Proc. IEEE Int. Conf. Acoust., Speech, Signal Process.*, Seoul, Republic of Korea, 2024, pp. 5855–5859. DOI: 10.1109/ICASSP48485.2024.10446701
- [15] Y. Akiyama, M. Vu, and K. Slavakis, "Nonparametric Bellman mappings for reinforcement learning: Application to robust adaptive filtering," *IEEE Trans. Signal Process.*, vol. 72, pp. 5644–5658, 2024. DOI: 10.1109/TSP.2024.3505266
- [16] N. Aronszajn, "Theory of reproducing kernels," *Trans. American Math. Society*, vol. 68, no. 3, pp. 337–404, 1950.
- [17] B. Schölkopf and A. J. Smola, *Learning with Kernels: Support Vector Machines, Regularization, Optimization, and Beyond*. MIT Press, 2002.
- [18] V. Mnih, K. Kavukcuoglu, D. Silver, A. Graves, I. Antonoglou, D. Wierstra, and M. A. Riedmiller, "Playing Atari with deep reinforcement learning," *CoRR*, vol. abs/1312.5602, 2013. arXiv: 1312.5602.
- [19] H. v. Hasselt, A. Guez, and D. Silver, "Deep reinforcement learning with double Q-learning," in *AAAI Conference on Artificial Intelligence*, Phoenix, Arizona: AAAI Press, 2016, pp. 2094–2100.
- [20] L.-J. Lin, "Reinforcement learning for robots using neural networks," Ph.D. dissertation, Carnegie Mellon University, USA, 1992.
- [21] M. Sato and S. Ishii, "Reinforcement learning based on on-line EM algorithm," in *Advance Neural Info. Process. Systems*, vol. 11, Denver, CO, USA: MIT Press, 1998, pp. 1052–1058.
- [22] Y. Engel, S. Mannor, and R. Meir, "Reinforcement learning with Gaussian processes," in *Proc. Int. Conf. Mach. Learn.*, Bonn, Germany: Association for Computing Machinery, 2005, pp. 201–208. DOI: 10.1145/1102351.1102377
- [23] A. Agostini and E. Celaya, "Reinforcement learning with a Gaussian mixture model," in *Proc. Int. Joint Conf. Neural Net.*, Barcelona, Spain, 2010, pp. 1–8. DOI: 10.1109/IJCNN.2010.5596306
- [24] A. Agostini and E. Celaya, "Online reinforcement learning using a probability density estimation," *Neural Comput.*, vol. 29, no. 1, pp. 220–246, Jan. 2017. DOI: 10.1162/NECO_a_00906
- [25] Y. Choi, K. Lee, and S. Oh, "Distributional deep reinforcement learning with a mixture of Gaussians," in *Proc. IEEE Int. Conf. Robot. Auto.*, Montreal, QC, Canada, 2019, pp. 9791–9797. DOI: 10.1109/ICRA.2019.8793505
- [26] D. Reynolds, "Gaussian mixture models," in *Encyclopedia of Biometrics*. Boston, MA: Springer US, 2009, pp. 659–663. DOI: 10.1007/978-0-387-73003-5_196
- [27] G. McLachlan and D. Peel, *Finite Mixture Models*. Wiley, 2000.
- [28] A. P. Dempster, N. M. Laird, and D. B. Rubin, "Maximum likelihood from incomplete data via the EM algorithm," *Journal of the Royal Statistical Society: Series B*, vol. 39, pp. 1–38, 1977.
- [29] M. A. T. Figueiredo and A. K. Jain, "Unsupervised learning of finite mixture models," *IEEE Trans. Pat. Ana. Mach. Intel.*, vol. 24, no. 3, pp. 381–396, 2002. DOI: 10.1109/34.990138
- [30] P.-A. Absil, R. Mahony, and R. Sepulchre, *Optimization Algorithms on Matrix Manifolds*. Princeton, NJ: Princeton University Press, 2008.
- [31] S. Wang, B. Zhu, C. Li, M. Wu, J. Zhang, W. Chu, and Y. Qi, "Riemannian proximal policy optimization," *Computer and Information Science*, vol. 13, no. 3, pp. 1–93, Aug. 2020.
- [32] R. S. Sutton, D. McAllester, S. Singh, and Y. Mansour, "Policy gradient methods for reinforcement learning with function approximation," in *Advance Neural Info. Process. Systems*, vol. 12, Denver, CO, USA: MIT Press, 1999, pp. 1057–1063.
- [33] J. Park and I. W. Sandberg, "Approximation and radial-basis-function networks," *Neural Comput.*, vol. 5, no. 2, pp. 305–316, 1993. DOI: 10.1162/neco.1993.5.2.305
- [34] M. Vu and K. Slavakis, "Riemannian Q-functions for policy iteration in reinforcement learning," in *European Signal Process. Conf.*, Isola delle Femmine, Palermo, Italy, Sep. 8–12, 2025, pp. 1672–1676.
- [35] H. H. Bauschke and P. L. Combettes, *Convex Analysis and Monotone Operator Theory in Hilbert Spaces*. New York, NY: Springer, 2011.
- [36] R. J. Williams and L. C. Baird III, "Tight performance bounds on greedy policies based on imperfect value functions," in *Tenth Yale Workshop on Adaptive and Learning Systems*, New Haven, CT, USA: Center for Systems Science, Yale University, 1994.
- [37] G. S. Kimeldorf and G. Wahba, "A correspondence between Bayesian estimation on stochastic processes and smoothing by splines," *The Annals of Mathematical Statistics*, vol. 41, no. 2, pp. 495–502, 1970. DOI: 10.1214/aoms/1177697089
- [38] T. Chen and H. Chen, "Universal approximation capability of EBF neural networks with arbitrary activation functions," *Circuits, Systems and Signal Processing*, vol. 15, no. 5, pp. 671–683, 1996. DOI: 10.1007/BF01188988
- [39] J. W. Robbin and D. A. Salamon, *Introduction to Differential Geometry*. Berlin: Springer, 2022.
- [40] D. Williams, *Probability with Martingales*. Cambridge University Press, 1991.
- [41] R. B. Ash and C. A. Doléans-Dade, *Probability and Measure Theory*, 2nd ed. Academic Press, 2000.
- [42] W. Rudin, *Real and Complex Analysis*, 3rd ed. New York: McGraw-Hill, 1987.
- [43] L. Malagò, L. Montrucchio, and G. Pistone, "Wasserstein Riemannian geometry of Gaussian densities," *Information Geometry*, vol. 1, no. 2, pp. 137–179, 2018. DOI: 10.1007/s41884-018-0014-4
- [44] R. Bobiti and M. Lazar, "A sampling approach to finding Lyapunov functions for nonlinear discrete-time systems," in *European Control Conference (ECC)*, Aalborg, Denmark, 2016, pp. 561–566. DOI: 10.1109/ECC.2016.7810344
- [45] N. Boumal, *An Introduction to Optimization on Smooth Manifolds*. USA: Cambridge University Press, 2023.
- [46] L. Prechelt, "Early stopping—but when?" In *Neural Networks: Tricks of the Trade: Second Edition*. Berlin, Heidelberg: Springer Berlin Heidelberg, 2012, pp. 53–67. DOI: 10.1007/978-3-642-35289-8_5
- [47] A. Antos, C. Szepesvári, and R. Munos, "Learning near-optimal policies with bellman-residual minimization based fitted policy iteration and a single sample path," in *Learning Theory*, Berlin, Heidelberg: Springer Berlin Heidelberg, 2006, pp. 574–588.
- [48] N. J. Ehsan Saleh, "Deterministic Bellman residual minimization," in *Advance Neural Info. Process. Systems*, in 2019.
- [49] D. E. Knuth, "Big Omicron and big Omega and big Theta," vol. 8, no. 2, 1976.
- [50] K. Doya, "Reinforcement learning in continuous time and space," *Neural Comput.*, vol. 12, no. 1, pp. 219–245, 2000. DOI: 10.1162/089976600300015961
- [51] A. W. Moore, "Efficient memory-based learning for robot control," University of Cambridge, Tech. Rep., 1990.
- [52] M. Spong, "The swing up control problem for the acrobat," *IEEE Control Systems Magazine*, vol. 15, no. 1, pp. 49–55, 1995. DOI: 10.1109/37.341864
- [53] Z. Wang, T. Schaul, M. Hessel, H. Van Hasselt, M. Lanctot, and N. De Freitas, "Dueling network architectures for deep reinforcement learning," in *Proc. Int. Conf. Mach. Learn.*, New York, NY, USA, 2016, pp. 1995–2003.
- [54] J. Schulman, F. Wolski, P. Dhariwal, A. Radford, and O. Klimov, "Proximal policy optimization algorithms," *CoRR*, vol. abs/1707.06347, 2017. arXiv: 1707.06347.
- [55] J. Bezanson, A. Edelman, S. Karpinski, and V. B. Shah, "Julia: A fresh approach to numerical computing," *SIAM Review*, vol. 59, no. 1, pp. 65–98, 2017. DOI: 10.1137/141000671
- [56] K. P. Badrinarath and D. Kalathil, "Robust reinforcement learning using least squares policy iteration with provable performance guarantees," in *Proc. Int. Conf. Mach. Learn.*, vol. 139, PMLR, Jul. 2021, pp. 511–520.
- [57] A. Geron, *Tiny-dqn*, <https://github.com/ageron/tiny-dqn>, 2017.
- [58] J. B. Conway, *A Course in Functional Analysis*, 2nd ed. Springer, 1990.
- [59] A. Pinkus, "Density in approximation theory," *Surveys in Approximation Theory*, vol. 1, pp. 1–45, 2005.

APPENDIX A
PROOF OF THEOREM 1

By the definition of $\mathcal{H}_{\mathbf{C}_k}^{\text{pre}}$ in (4a), $Q_k = \sum_{l=1}^{L_k} \alpha_{kl} \mathcal{G}(\cdot | \mathbf{m}_{kl}, \mathbf{C}_k)$, for distinct $\{\mathbf{m}_{kl}\}_{l=1}^{L_k}$, that is, $\mathbf{m}_{kl} \neq \mathbf{m}_{k'l'}$, $\forall (l, l') \in \overline{1, L_k}^2$ with $l < l'$, for nonzero $\{\alpha_{kl}\}_{l=1}^{L_k} \subset \mathbb{R}$ and $L_k \in \mathbb{N}_*$. As such, for any \mathbf{z} ,

$$\begin{aligned} 0 &= \sum_{k=1}^K \beta_k \sum_{l=1}^{L_k} \alpha_{kl} \mathcal{G}(\mathbf{z} | \mathbf{m}_{kl}, \mathbf{C}_k) \\ &= \sum_{k=1}^K \sum_{l=1}^{L_k} \overbrace{\beta_k \alpha_{kl}}^{\vartheta_{kl}} \mathcal{G}(\mathbf{z} | \mathbf{m}_{kl}, \mathbf{C}_k) \\ &= \sum_{k=1}^K \sum_{l=1}^{L_k} \vartheta_{kl} \exp(-\|\mathbf{z}\|_{\mathbf{C}_k}^2 + 2\langle \mathbf{z} | \mathbf{m}_{kl} \rangle_{\mathbf{C}_k^{-1}} \\ &\quad - \|\mathbf{m}_{kl}\|_{\mathbf{C}_k}^2), \end{aligned} \quad (22)$$

where

$$\begin{aligned} \|\mathbf{z}\|_{\mathbf{C}_k}^2 &:= \mathbf{z}^\top \mathbf{C}_k^{-1} \mathbf{z}, \quad \|\mathbf{m}_{kl}\|_{\mathbf{C}_k}^2 := \mathbf{m}_{kl}^\top \mathbf{C}_k^{-1} \mathbf{m}_{kl}, \\ \langle \mathbf{z} | \mathbf{m}_{kl} \rangle_{\mathbf{C}_k^{-1}} &:= \mathbf{z}^\top \mathbf{C}_k^{-1} \mathbf{m}_{kl}. \end{aligned}$$

Define now the index set

$$\mathcal{J}_0 := \{(k, k', l, l') | \mathbf{C}_k^{-1} \mathbf{m}_{kl} \neq \mathbf{C}_{k'}^{-1} \mathbf{m}_{k'l'}, k \leq k', l \leq l'\},$$

and choose $\mathbf{z}_\# \in \mathbb{R}^{D_z}$ such that

$$\begin{aligned} \mathbf{z}_\# \notin \bigcup_{k < k'} \{\mathbf{z} \in \mathbb{R}^{D_z} | \mathbf{z}^\top (\mathbf{C}_k^{-1} - \mathbf{C}_{k'}^{-1}) \mathbf{z} = 0\} \\ \cup \bigcup_{(k, k', l, l') \in \mathcal{J}_0} \{\mathbf{z} \in \mathbb{R}^{D_z} | \mathbf{z}^\top (\mathbf{C}_k^{-1} \mathbf{m}_{kl} - \mathbf{C}_{k'}^{-1} \mathbf{m}_{k'l'}) = 0\}. \end{aligned} \quad (23)$$

The union in (23) involves a finite number of quadric hypersurfaces $\{\mathbf{z} \in \mathbb{R}^{D_z} | \mathbf{z}^\top (\mathbf{C}_k^{-1} - \mathbf{C}_{k'}^{-1}) \mathbf{z} = 0\}$ and hyperplanes $\{\mathbf{z} \in \mathbb{R}^{D_z} | \mathbf{z}^\top (\mathbf{C}_k^{-1} \mathbf{m}_{kl} - \mathbf{C}_{k'}^{-1} \mathbf{m}_{k'l'}) = 0\}$, which are smooth $(D_z - 1)$ -dimensional manifolds that cross the origin [39, Example 2.2.5]. Such a finite number of smooth manifolds cannot cover the whole ambient space \mathbb{R}^{D_z} , and a $\mathbf{z}_\#$ which satisfies (23) can always be chosen.

Let now $\mathbf{z} = t\mathbf{z}_\#$, with $t \in \mathbb{R}_{++}$, so that (22) becomes

$$\begin{aligned} 0 &= \sum_{k=1}^K \sum_{l=1}^{L_k} \vartheta_{kl} \exp(-t^2 \|\mathbf{z}_\#\|_{\mathbf{C}_k}^2 + 2t \langle \mathbf{z}_\# | \mathbf{m}_{kl} \rangle_{\mathbf{C}_k^{-1}} \\ &\quad - \|\mathbf{m}_{kl}\|_{\mathbf{C}_k}^2). \end{aligned} \quad (24)$$

Because of (23), all $\{\|\mathbf{z}_\#\|_{\mathbf{C}_k}^2\}_{k=1}^K$ are distinct, so that it can be assumed, w.l.o.g., that $\|\mathbf{z}_\#\|_{\mathbf{C}_1}^2 < \|\mathbf{z}_\#\|_{\mathbf{C}_k}^2$, $\forall k \in \overline{2, K}$. Dividing both sides of (24) by $\exp(-t^2 \|\mathbf{z}_\#\|_{\mathbf{C}_1}^2)$ yields

$$\begin{aligned} 0 &= \sum_{l=1}^{L_1} \vartheta_{1l} \exp(2t \langle \mathbf{z}_\# | \mathbf{m}_{1l} \rangle_{\mathbf{C}_1^{-1}} - \|\mathbf{m}_{1l}\|_{\mathbf{C}_1}^2) \\ &\quad + \sum_{k=2}^K \sum_{l=1}^{L_k} \vartheta_{kl} \exp(-t^2 (\|\mathbf{z}_\#\|_{\mathbf{C}_k}^2 - \|\mathbf{z}_\#\|_{\mathbf{C}_1}^2) \\ &\quad + 2t \langle \mathbf{z}_\# | \mathbf{m}_{kl} \rangle_{\mathbf{C}_k^{-1}} - \|\mathbf{m}_{kl}\|_{\mathbf{C}_k}^2). \end{aligned} \quad (25)$$

Again because of (23), all $\{\langle \mathbf{z}_\# | \mathbf{m}_{1l} \rangle_{\mathbf{C}_1^{-1}}\}_{l=1}^{L_1}$ are distinct, so that $\exists l_\# \in \overline{1, L_1}$ with $\langle \mathbf{z}_\# | \mathbf{m}_{1l_\#} \rangle_{\mathbf{C}_1^{-1}} > \langle \mathbf{z}_\# | \mathbf{m}_{1l} \rangle_{\mathbf{C}_1^{-1}}$,

$\forall l \in \overline{1, L_1} \setminus \{l_\#\}$. Dividing both sides of (25) by $\exp(2t \langle \mathbf{z}_\# | \mathbf{m}_{1l_\#} \rangle_{\mathbf{C}_1^{-1}})$ yields

$$\begin{aligned} 0 &= \vartheta_{1l_\#} \exp(-\|\mathbf{m}_{1l_\#}\|_{\mathbf{C}_1}^2) \\ &\quad + \sum_{l \in \overline{1, L_1} \setminus \{l_\#\}} \vartheta_{1l} \exp(+2t \langle \mathbf{z}_\# | \mathbf{m}_{1l} - \mathbf{m}_{1l_\#} \rangle_{\mathbf{C}_1^{-1}} \\ &\quad - \|\mathbf{m}_{1l}\|_{\mathbf{C}_1}^2) \\ &\quad + \sum_{k=2}^K \sum_{l=1}^{L_k} \vartheta_{kl} \exp(-t^2 (\|\mathbf{z}_\#\|_{\mathbf{C}_k}^2 - \|\mathbf{z}_\#\|_{\mathbf{C}_1}^2) \\ &\quad + 2t (\langle \mathbf{z}_\# | \mathbf{m}_{kl} \rangle_{\mathbf{C}_k^{-1}} - \langle \mathbf{z}_\# | \mathbf{m}_{1l_\#} \rangle_{\mathbf{C}_1^{-1}} \\ &\quad - \|\mathbf{m}_{kl}\|_{\mathbf{C}_k}^2)). \end{aligned} \quad (26)$$

It can be now readily verified that $\lim_{t \rightarrow +\infty} \exp(2t \langle \mathbf{z}_\# | \mathbf{m}_{1l} - \mathbf{m}_{1l_\#} \rangle_{\mathbf{C}_1^{-1}}) = \exp(-\infty) = 0$, and

$$\begin{aligned} \lim_{t \rightarrow +\infty} \exp(-t^2 (\|\mathbf{z}_\#\|_{\mathbf{C}_k}^2 - \|\mathbf{z}_\#\|_{\mathbf{C}_1}^2) \\ + 2t (\langle \mathbf{z}_\# | \mathbf{m}_{kl} \rangle_{\mathbf{C}_k^{-1}} - \langle \mathbf{z}_\# | \mathbf{m}_{1l_\#} \rangle_{\mathbf{C}_1^{-1}})) \\ = \exp(-\infty) = 0. \end{aligned}$$

Therefore, applying $\lim_{t \rightarrow +\infty}$ to both sides of (26) yields

$$\begin{aligned} 0 &= \vartheta_{1l_\#} \exp(-\|\mathbf{m}_{1l_\#}\|_{\mathbf{C}_1}^2) \Rightarrow 0 = \vartheta_{1l_\#} = \beta_1 \alpha_{1l_\#} \\ &\Rightarrow 0 = \beta_1, \end{aligned}$$

because $\alpha_{1l_\#}$ is nonzero. Consequently, $0 = \sum_{k=1}^K \beta_k Q_k \Rightarrow 0 = \sum_{k=2}^K \beta_k Q_k$. Repeating the previous arguments leads to $0 = \beta_k$, $\forall k \in \overline{2, K-1}$. Finally, $0 = \beta_K Q_K \Rightarrow 0 = \beta_K$, because Q_K is nonzero. This completes the proof.

APPENDIX B
PROOF OF THEOREM 3

First, notice that for an arbitrarily fixed $K \in \mathbb{N}_*$, any \mathcal{Q} -function in \mathcal{Q}_K belongs to $C(\mathfrak{Z})$; hence, $\cup_{K \in \mathbb{N}_*} \mathcal{Q}_K \subset C(\mathfrak{Z})$. Moreover, it can be readily verified by the definition (7) that $\cup_{K \in \mathbb{N}_*} \mathcal{Q}_K$ is a linear vector space. Notice also that $\forall (\mathbf{m}_1, \mathbf{C}_1), (\mathbf{m}_2, \mathbf{C}_2) \in \mathbb{R}^{D_z} \times \mathbb{S}_{++}^{D_z}$ the point-wise multiplication

$$\begin{aligned} \mathcal{G}(\mathbf{z} | \mathbf{m}_1, \mathbf{C}_1) \cdot \mathcal{G}(\mathbf{z} | \mathbf{m}_2, \mathbf{C}_2) \\ = \exp(-\mathbf{m}_1^\top \mathbf{C}_1^{-1} \mathbf{m}_1 - \mathbf{m}_2^\top \mathbf{C}_2^{-1} \mathbf{m}_2 + \mathbf{m}^\top (\mathbf{C}_1^{-1} + \mathbf{C}_2^{-1}) \mathbf{m}) \\ \cdot \mathcal{G}(\mathbf{z} | \mathbf{m}, \mathbf{C}) \in \cup_{K \in \mathbb{N}_*} \mathcal{Q}_K, \end{aligned} \quad (27)$$

where

$$\begin{aligned} \mathbf{m} &:= (\mathbf{C}_1^{-1} + \mathbf{C}_2^{-1})^{-1} (\mathbf{C}_1^{-1} \mathbf{m}_1 + \mathbf{C}_2^{-1} \mathbf{m}_2), \\ \mathbf{C} &:= (\mathbf{C}_1^{-1} + \mathbf{C}_2^{-1})^{-1}. \end{aligned}$$

Result (27) together with the previous discussion render $\cup_{K \in \mathbb{N}_*} \mathcal{Q}_K$ a subalgebra [58] of $C(\mathfrak{Z})$, which, however, does not include the unit/identity element $1 \in C(\mathfrak{Z})$ w.r.t. point-wise multiplication, defined as the constant function with value equal to 1 on \mathfrak{Z} . Nevertheless, 1 belongs to the closure of $\cup_{K \in \mathbb{N}_*} \mathcal{Q}_K$ w.r.t. the topology induced by $\|\cdot\|_\infty$, as the following discussion suggests: with $\Delta := \sup_{(\mathbf{z}, \mathbf{m}) \in \mathfrak{Z}^2} \|\mathbf{z} - \mathbf{m}\| < +\infty$, let the sequence of Gaussians $(\mathcal{G}(\cdot | \mathbf{m}, k\mathbf{I}_{D_z}))_{k \in \mathbb{N}_*} \subset \cup_{K \in \mathbb{N}_*} \mathcal{Q}_K$, for some $\mathbf{m} \in \mathfrak{Z}$, and notice that

$$\forall \mathbf{z} \in \mathfrak{Z}, \quad |1 - \mathcal{G}(\mathbf{z} | \mathbf{m}, k\mathbf{I}_{D_z})| = 1 - \mathcal{G}(\mathbf{z} | \mathbf{m}, k\mathbf{I}_{D_z})$$

$$\begin{aligned}
&= 1 - \exp(-\|\mathbf{z} - \mathbf{m}\|^2/k) \\
&\leq 1 - \exp(-\Delta^2/k) \\
\Rightarrow \quad &\|1 - \mathcal{G}(\cdot | \mathbf{m}, k\mathbf{I}_{D_z})\|_\infty \\
&= \sup_{\mathbf{z} \in \mathfrak{Z}} |1 - \mathcal{G}(\mathbf{z} | \mathbf{m}, k\mathbf{I}_{D_z})| \\
&\leq 1 - \exp(-\Delta^2/k) \\
\Rightarrow \quad &\lim_{k \rightarrow \infty} \|1 - \mathcal{G}(\cdot | \mathbf{m}, k\mathbf{I}_{D_z})\|_\infty = 0.
\end{aligned}$$

Furthermore, for any $\mathbf{z}, \mathbf{m} \in \mathfrak{Z}$, there always exists a Q-function $Q \in \cup_{K \in \mathbb{N}_*} \mathcal{Q}_K$ which “separates” the points \mathbf{z} and \mathbf{m} , i.e., $Q(\mathbf{z}) \neq Q(\mathbf{m})$, and at the same time $Q(\mathbf{m}) \neq 0$ —choose, for example, $Q := \mathcal{G}(\cdot | \mathbf{m}, \mathbf{C})$, for some $\mathbf{C} \in \mathbb{S}_{++}^{D_z}$.

The preceding discussion indicates that the sufficient conditions of the Stone-Weierstrass theorem [59, Thm. 4.1] are satisfied—the proof of which does not require the unit element 1 to be included in the subalgebra—thereby ensuring that the statement of Theorem 3(i) holds true.

With regards to the proof of Theorem 3(ii), consider an arbitrarily fixed $Q \in L_2(\mathfrak{P})$ and an arbitrarily small $\varepsilon \in \mathbb{R}_{++}$. Under Assumption 2 and according to [42, Thm. 3.14, pp. 69], there exists $Q' \in C(\mathfrak{Z})$ s.t. $\|Q - Q'\|_{L_2(\mathfrak{P})} \leq \varepsilon/2$. Furthermore, by Theorem 3(i) there exists $Q'' \in \cup_{K \in \mathbb{N}_*} \mathcal{Q}_K$ s.t. $\|Q' - Q''\|_\infty \leq \varepsilon/2$. Hence,

$$\begin{aligned}
\|Q - Q''\|_{L_2(\mathfrak{P})} &\leq \|Q - Q'\|_{L_2(\mathfrak{P})} + \|Q' - Q''\|_{L_2(\mathfrak{P})} \\
&\leq \frac{\varepsilon}{2} + \left(\int_{\mathfrak{Z}} |Q'(\mathbf{z}) - Q''(\mathbf{z})|^2 \mathfrak{P}(d\mathbf{z}) \right)^{1/2} \\
&\leq \frac{\varepsilon}{2} + \left(\|Q' - Q''\|_\infty^2 \int_{\mathfrak{Z}} \mathfrak{P}(d\mathbf{z}) \right)^{1/2} \\
&= \frac{\varepsilon}{2} + \|Q' - Q''\|_\infty \leq \frac{\varepsilon}{2} + \frac{\varepsilon}{2} \leq \varepsilon,
\end{aligned}$$

which establishes the proof of Theorem 3(ii).

The following proof of Theorem 3(iii) extends that of [38, Thm. 4] to the case where the covariance matrices of the Gaussians are not necessarily diagonal.

Assume for a contradiction that $\cup_{K \in \mathbb{N}_*} \mathcal{Q}_K$ is not dense in $L_2(\mathbb{R}^{D_z})$. First, recall the well-known fact that $\mathcal{G}(\cdot | \mathbf{m}, \mathbf{C}) \in L_2(\mathbb{R}^{D_z})$, $\forall (\mathbf{m}, \mathbf{C}) \in \mathbb{R}^{D_z} \times \mathbb{S}_{++}^{D_z}$. Hence, $\cup_{K \in \mathbb{N}_*} \mathcal{Q}_K$ is a linear subspace of $L_2(\mathbb{R}^{D_z})$. The hypothesis on the non-density and the Hahn-Banach theorem [58, Chapter III, Cor. 6.14] suggest that there exists a *nonzero* continuous linear functional $l(\cdot)$ on $L_2(\mathbb{R}^{D_z})$ such that $l(Q) = 0$, $\forall Q \in \cup_{K \in \mathbb{N}_*} \mathcal{Q}_K$. Consequently, by the Riesz representation theorem [58, Chapter I, Cor. 3.5], there exists a *nonzero* $R(\cdot) \in L_2(\mathbb{R}^{D_z})$ such that $\forall Q \in \cup_{K \in \mathbb{N}_*} \mathcal{Q}_K$,

$$l(Q) = \int Q(\mathbf{z})R(\mathbf{z})d\mathbf{z} = \langle Q | R \rangle_{L_2(\mathbb{R}^{D_z})} = 0, \quad (28)$$

which holds true also for the special Q-function $\mathcal{G}(\cdot | \mathbf{m}, \mathbf{C}) \in \cup_{K \in \mathbb{N}_*} \mathcal{Q}_K$, $\forall (\mathbf{m}, \mathbf{C}) \in \mathbb{R}^{D_z} \times \mathbb{S}_{++}^{D_z}$:

$$\int \mathcal{G}(\mathbf{z} | \mathbf{m}, \mathbf{C})R(\mathbf{z})d\mathbf{z} = 0.$$

Now, consider *any* function $W(\cdot)$ from the set of all (Schwartz) rapidly decreasing functions $S(\mathbb{R}^{D_z}) \subset L_2(\mathbb{R}^{D_z})$ [58, Chapter X, Def. 6.3] to obtain

$$\int W(\mathbf{m}) \left(\int \mathcal{G}(\mathbf{z} | \mathbf{m}, \mathbf{C})R(\mathbf{z})d\mathbf{z} \right) d\mathbf{m} = 0. \quad (29)$$

Define $\mathbf{x} := \mathbf{C}^{-1/2}(\mathbf{z} - \mathbf{m})$. Then, $(\mathbf{z} - \mathbf{m})^\top \mathbf{C}^{-1}(\mathbf{z} - \mathbf{m}) = \|\mathbf{x}\|^2$. Notice that $\mathcal{G}(\cdot | \mathbf{0}, \mathbf{I})$ is also a rapidly decreasing function, and that by dividing the nonzero $|\det \mathbf{C}^{1/2}|$ from both sides, Fubini’s theorem [58] and (29) yields

$$\begin{aligned}
&\int W(\mathbf{m}) \int \mathcal{G}(\mathbf{x} | \mathbf{0}, \mathbf{I}) R(\mathbf{C}^{1/2}\mathbf{x} + \mathbf{m}) d\mathbf{x} d\mathbf{m} \\
&= \int \mathcal{G}(\mathbf{x} | \mathbf{0}, \mathbf{I}) \left(\int W(\mathbf{m}) R(\mathbf{C}^{1/2}\mathbf{x} + \mathbf{m}) d\mathbf{m} \right) d\mathbf{x} \\
&= \int \mathcal{G}(\mathbf{x} | \mathbf{0}, \mathbf{I}) \left(\int W(\mathbf{m}) \check{R}(-\mathbf{C}^{1/2}\mathbf{x} - \mathbf{m}) d\mathbf{m} \right) d\mathbf{x} \\
&= \int \mathcal{G}(\mathbf{x} | \mathbf{0}, \mathbf{I}) (W * \check{R})(-\mathbf{C}^{1/2}\mathbf{x}) d\mathbf{x} = 0, \quad (30)
\end{aligned}$$

where $\check{R}(\cdot) := R(-\cdot)$ and $(W * \check{R})(\cdot)$ denotes the convolution of W and \check{R} [58].

With $\mathcal{F}[\cdot]$ denoting the D_z -dimensional Fourier transform, let $\mathcal{G}(\omega) := \mathcal{F}[\mathcal{G}(\cdot | \mathbf{0}, \mathbf{I})](\omega)$, which is well known to be isotropic, $\mathcal{W}(\omega) := \mathcal{F}[W(\cdot)](\omega)$, $\check{\mathcal{R}}(\omega) := \mathcal{F}[\check{R}(\cdot)](\omega)$. Recall also that the Fourier transform is unitary, i.e., $\mathcal{F}^* = \mathcal{F}^{-1}$, where \mathcal{F}^* is the adjoint operator of \mathcal{F} [58, Chapter X, Thm. 6.17]. Now, by (30),

$$\begin{aligned}
0 &= \langle \mathcal{G}(\cdot | \mathbf{0}, \mathbf{I}) | (W * \check{R})(-\mathbf{C}^{1/2}\cdot) \rangle_{L_2(\mathbb{R}^{D_z})} \\
&= \langle \mathcal{F}^{-1} \mathcal{F}[\mathcal{G}(\cdot | \mathbf{0}, \mathbf{I})] | (W * \check{R})(-\mathbf{C}^{1/2}\cdot) \rangle_{L_2(\mathbb{R}^{D_z})} \\
&= \langle \mathcal{F}[\mathcal{G}(\cdot | \mathbf{0}, \mathbf{I})] | \mathcal{F}^{-*}[(W * \check{R})(-\mathbf{C}^{1/2}\cdot)] \rangle_{L_2(\mathbb{R}^{D_z})} \\
&= \langle \mathcal{F}[\mathcal{G}(\cdot | \mathbf{0}, \mathbf{I})] | \mathcal{F}[(W * \check{R})(-\mathbf{C}^{1/2}\cdot)] \rangle_{L_2(\mathbb{R}^{D_z})} \\
&= \int \mathcal{G}(\omega) \mathcal{W}(-\mathbf{C}^{-1/2}\omega) \check{\mathcal{R}}(-\mathbf{C}^{-1/2}\omega) d\omega \\
&= \int \mathcal{G}(-\mathbf{C}^{1/2}\omega') \mathcal{W}(\omega') \check{\mathcal{R}}(\omega') d\omega' \quad (\omega' := -\mathbf{C}^{-1/2}\omega) \\
&= \langle \mathcal{W}(\cdot) | \mathcal{G}(\mathbf{C}^{1/2}\cdot) \check{\mathcal{R}}(\cdot) \rangle_{L_2(\mathbb{R}^{D_z})} \\
&= \langle \mathcal{F}[W](\cdot) | \mathcal{G}(\mathbf{C}^{1/2}\cdot) \check{\mathcal{R}}(\cdot) \rangle_{L_2(\mathbb{R}^{D_z})} \\
&= \langle W | \mathcal{F}^*[\mathcal{G}(\mathbf{C}^{1/2}\cdot) \check{\mathcal{R}}(\cdot)] \rangle_{L_2(\mathbb{R}^{D_z})} \\
&= \langle W | \mathcal{F}^{-1}[\mathcal{G}(\mathbf{C}^{1/2}\cdot) \check{\mathcal{R}}(\cdot)] \rangle_{L_2(\mathbb{R}^{D_z})}, \quad (31)
\end{aligned}$$

where $\mathcal{G}(-\mathbf{C}^{1/2}\cdot) = \mathcal{G}(\mathbf{C}^{1/2}\cdot)$ because $\mathcal{G}(\cdot)$ is isotropic, and $\mathcal{G}(\mathbf{C}^{1/2}\cdot) \check{\mathcal{R}}(\cdot) \in L_2(\mathbb{R}^{D_z})$ because $\mathcal{G}(\mathbf{C}^{1/2}\cdot)$ is bounded and $\check{\mathcal{R}}(\cdot) \in L_2(\mathbb{R}^{D_z})$. Note that (31) holds true for any $W \in S(\mathbb{R}^{D_z})$.

Owing to the fact that $S(\mathbb{R}^{D_z})$ is dense in $L_2(\mathbb{R}^{D_z})$ [58, Chapter X, Prop. 6.5], consider a sequence $(W_m)_{m \in \mathbb{N}} \in S(\mathbb{R}^{D_z})$ such that $\lim_{m \rightarrow \infty} W_m = \mathcal{F}^{-1}[\mathcal{G}(\mathbf{C}^{1/2}\cdot) \check{\mathcal{R}}(\cdot)]$ in the strong topology of $L_2(\mathbb{R}^{D_z})$. It can be therefore deduced by (31) that

$$\begin{aligned}
&\|\mathcal{G}(\mathbf{C}^{1/2}\cdot) \check{\mathcal{R}}(\cdot)\|_{L_2(\mathbb{R}^{D_z})}^2 \\
&= \langle \mathcal{G}(\mathbf{C}^{1/2}\cdot) \check{\mathcal{R}}(\cdot) | \mathcal{G}(\mathbf{C}^{1/2}\cdot) \check{\mathcal{R}}(\cdot) \rangle_{L_2(\mathbb{R}^{D_z})} \\
&= \langle \mathcal{F} \mathcal{F}^{-1}[\mathcal{G}(\mathbf{C}^{1/2}\cdot) \check{\mathcal{R}}(\cdot)] | \mathcal{G}(\mathbf{C}^{1/2}\cdot) \check{\mathcal{R}}(\cdot) \rangle_{L_2(\mathbb{R}^{D_z})} \\
&= \langle \mathcal{F}^{-1}[\mathcal{G}(\mathbf{C}^{1/2}\cdot) \check{\mathcal{R}}(\cdot)] | \mathcal{F}^{-1}[\mathcal{G}(\mathbf{C}^{1/2}\cdot) \check{\mathcal{R}}(\cdot)] \rangle_{L_2(\mathbb{R}^{D_z})} \\
&= \langle \lim_{m \rightarrow \infty} W_m | \mathcal{F}^{-1}[\mathcal{G}(\mathbf{C}^{1/2}\cdot) \check{\mathcal{R}}(\cdot)] \rangle_{L_2(\mathbb{R}^{D_z})} \\
&= \lim_{m \rightarrow \infty} \langle W_m | \mathcal{F}^{-1}[\mathcal{G}(\mathbf{C}^{1/2}\cdot) \check{\mathcal{R}}(\cdot)] \rangle_{L_2(\mathbb{R}^{D_z})} = 0.
\end{aligned}$$

Consequently, $\mathcal{G}(\mathbf{C}^{1/2}\cdot) \check{\mathcal{R}}(\cdot) = 0$, almost everywhere (a.e.) with respect to the Lebesgue measure $\Rightarrow \check{\mathcal{R}} = 0$, a.e., because $\mathcal{G}(\mathbf{C}^{1/2}\cdot)$ is nonzero everywhere, and thus $\check{R} = \mathcal{F}^{-1}[\check{\mathcal{R}}] = 0$,

a.e. Hence, $R(\cdot) = \tilde{R}(\cdot) = 0$, a.e., which contradicts the initial hypothesis that R is nonzero, asserting Theorem 3(iii).

APPENDIX C PROOF OF PROPOSITION 4

For an arbitrarily fixed $\epsilon \in \mathbb{R}_{++}$, there exists $Q \in C(3)$ s.t.

$$\hat{\mathcal{L}}_\mu[T](Q) \leq \inf_{Q' \in C(3)} \hat{\mathcal{L}}_\mu[T](Q') + \epsilon.$$

Define $\forall t \in \overline{1, T}$ the function

$$l_t: \mathbb{R}^2 \rightarrow \mathbb{R}_+: (q'_t, q_t) \mapsto l_t(q'_t, q_t) := (g_t + \alpha q'_t - q_t)^2,$$

which is continuous everywhere in \mathbb{R}^2 , and hence continuous at $(Q(\mathbf{z}'_t), Q(\mathbf{z}_t))$. Thus, there exists a sufficiently small $\delta_t \in \mathbb{R}_{++}$ s.t.

$$\begin{aligned} & \| (q'_t, q_t) - (Q(\mathbf{z}'_t), Q(\mathbf{z}_t)) \|_{\mathbb{R}^2} \leq \delta_t \\ \Rightarrow l_t(q'_t, q_t) & \leq l_t(Q(\mathbf{z}'_t), Q(\mathbf{z}_t)) + \epsilon \\ & = [g_t + \alpha Q(\mathbf{z}'_t) - Q(\mathbf{z}_t)]^2 + \epsilon. \end{aligned} \quad (32)$$

Define now $\delta := \min_{t \in \overline{1, T}} \delta_t$. By Theorem 3(i), there exists $\tilde{Q} \in \cup_{K \in \mathbb{N}_*} \mathcal{Q}_K$ s.t. $\|\tilde{Q} - Q\|_\infty \leq \delta/\sqrt{2}$, and consequently, $\forall t \in \overline{1, T}$,

$$|\tilde{Q}(\mathbf{z}'_t) - Q(\mathbf{z}'_t)| \leq \delta/\sqrt{2}, \quad |\tilde{Q}(\mathbf{z}_t) - Q(\mathbf{z}_t)| \leq \delta/\sqrt{2}.$$

Then, the tuple $(q'_t, q_t) := (\tilde{Q}(\mathbf{z}'_t), \tilde{Q}(\mathbf{z}_t))$ satisfies the sufficient condition in (32), and hence,

$$\begin{aligned} [g_t + \alpha \tilde{Q}(\mathbf{z}'_t) - \tilde{Q}(\mathbf{z}_t)]^2 & = l_t(\tilde{Q}(\mathbf{z}'_t), \tilde{Q}(\mathbf{z}_t)) \\ & \leq [g_t + \alpha Q(\mathbf{z}'_t) - Q(\mathbf{z}_t)]^2 + \epsilon. \end{aligned}$$

Summing up all previous terms $\forall t \in \overline{1, T}$, and dividing finally by T yields

$$\begin{aligned} & \inf_{\tilde{Q}' \in \cup_{K \in \mathbb{N}_*} \mathcal{Q}_K} \hat{\mathcal{L}}_\mu[T](\tilde{Q}') \\ & \leq \hat{\mathcal{L}}_\mu[T](\tilde{Q}) = \frac{1}{T} \sum_{t=1}^T [g_t + \alpha \tilde{Q}(\mathbf{z}'_t) - \tilde{Q}(\mathbf{z}_t)]^2 \\ & \leq \frac{1}{T} \sum_{t=1}^T [g_t + \alpha Q(\mathbf{z}'_t) - Q(\mathbf{z}_t)]^2 + \epsilon \\ & = \hat{\mathcal{L}}_\mu[T](Q) + \epsilon \leq \inf_{Q' \in C(3)} \hat{\mathcal{L}}_\mu[T](Q') + 2\epsilon. \end{aligned}$$

Because ϵ was chosen arbitrarily, the previous discussion leads to $\inf_{Q \in \cup_{K \in \mathbb{N}_*} \mathcal{Q}_K} \hat{\mathcal{L}}_\mu[T](Q) \leq \inf_{Q \in C(3)} \hat{\mathcal{L}}_\mu[T](Q)$. Moreover, because $\cup_{K \in \mathbb{N}_*} \mathcal{Q}_K \subset C(3)$, $\inf_{Q \in C(3)} \hat{\mathcal{L}}_\mu[T](Q) \leq \inf_{Q \in \cup_{K \in \mathbb{N}_*} \mathcal{Q}_K} \hat{\mathcal{L}}_\mu[T](Q)$, which completes the proof.

APPENDIX D DERIVATION OF GRADIENTS IN (18)

To simplify notation in the following proofs, $\mathcal{G}(\cdot | \mathbf{m}_k, \mathbf{C}_k)$ will be written as $\mathcal{G}_k(\cdot)$ or $\mathcal{G}_{\mathbf{C}_k}(\cdot)$; the hyperparameter T will be suppressed in the loss notation, and the superscript (j) will likewise be omitted. The derivation of (18a) is straightforward and therefore skipped.

A. Derivation of (18b)

The standard chain rule of differentiation suggests that

$$\begin{aligned} & \frac{\partial \hat{\mathcal{L}}_\mu}{\partial \mathbf{m}_k} \\ & = \frac{1}{T} \sum_{t=1}^T \frac{\partial}{\partial \mathbf{m}_k} \left[g_t + \sum_{i=1}^K \xi_i (\alpha \mathcal{G}_i(\mathbf{z}'_t) - \mathcal{G}_i(\mathbf{z}_t)) \right]^2 \\ & = \frac{1}{T} \sum_{t=1}^T 2\delta_t \xi_k \frac{\partial}{\partial \mathbf{m}_k} (\alpha \mathcal{G}_k(\mathbf{z}'_t) - \mathcal{G}_k(\mathbf{z}_t)) \\ & = \frac{1}{T} \sum_{t=1}^T 2\delta_t \xi_k \left[2\alpha \mathcal{G}_k(\mathbf{z}'_t) \cdot \mathbf{C}_k^{-1}(\mathbf{z}'_t - \mathbf{m}_k) \right. \\ & \quad \left. - 2\mathcal{G}_k(\mathbf{z}_t) \cdot \mathbf{C}_k^{-1}(\mathbf{z}_t - \mathbf{m}_k) \right] \\ & = \frac{1}{T} \sum_{t=1}^T 4\delta_t \xi_k \mathbf{C}_k^{-1} \mathbf{d}_{tk}, \end{aligned}$$

which establishes (18b).

B. Derivation of (18c) and (18d)

The (partial) derivative of the loss $\hat{\mathcal{L}}_\mu$ with respect to \mathbf{C}_k , at the point Ω and along an arbitrarily fixed direction $\Gamma \in T_{\mathbf{C}_k} \mathbb{S}_{++}^{D_z} = \mathbb{S}^{D_z}$, together with the chain rule of differentiation and the fact that the derivative of the inverse matrix function $\text{inv}: \mathbb{S}_{++}^{D_z} \rightarrow \mathbb{S}_{++}^{D_z}: \mathbf{C} \mapsto \text{inv}(\mathbf{C}) := \mathbf{C}^{-1}$ along Γ is $\text{D inv}(\mathbf{C})[\Gamma] = -\mathbf{C}^{-1} \Gamma \mathbf{C}^{-1}$ [30, Appendix A.5], yields

$$\begin{aligned} & \text{D}_{\mathbf{C}_k} \hat{\mathcal{L}}_\mu(\Omega)[\Gamma] \\ & = \frac{1}{T} \sum_{t=1}^T \text{D}_{\mathbf{C}_k} \left(\left[g_t + \sum_{i=1}^K \xi_i (\alpha \mathcal{G}_i(\mathbf{z}'_t) - \mathcal{G}_i(\mathbf{z}_t)) \right]^2 \right) [\Gamma] \\ & = \frac{1}{T} \sum_{t=1}^T 2\delta_t \xi_k \left[-\alpha \mathcal{G}_k(\mathbf{z}'_t) (\mathbf{z}'_t - \mathbf{m}_k)^\top \text{D inv}(\mathbf{C}_k)[\Gamma] (\mathbf{z}'_t - \mathbf{m}_k) \right. \\ & \quad \left. + \mathcal{G}_k(\mathbf{z}_t) (\mathbf{z}_t - \mathbf{m}_k)^\top \text{D inv}(\mathbf{C}_k)[\Gamma] (\mathbf{z}_t - \mathbf{m}_k) \right] \\ & = \frac{1}{T} \sum_{t=1}^T 2\delta_t \xi_k \left[\alpha \mathcal{G}_k(\mathbf{z}'_t) (\mathbf{z}'_t - \mathbf{m}_k)^\top \mathbf{C}_k^{-1} \Gamma \mathbf{C}_k^{-1} (\mathbf{z}'_t - \mathbf{m}_k) \right. \\ & \quad \left. - \mathcal{G}_k(\mathbf{z}_t) (\mathbf{z}_t - \mathbf{m}_k)^\top \mathbf{C}_k^{-1} \Gamma \mathbf{C}_k^{-1} (\mathbf{z}_t - \mathbf{m}_k) \right] \\ & = \frac{1}{T} \sum_{t=1}^T 2\delta_t \xi_k \text{tr} \left(\mathbf{C}_k^{-1} \left[\alpha \mathcal{G}_k(\mathbf{z}'_t) (\mathbf{z}'_t - \mathbf{m}_k) (\mathbf{z}'_t - \mathbf{m}_k)^\top \right. \right. \\ & \quad \left. \left. - \mathcal{G}_k(\mathbf{z}_t) (\mathbf{z}_t - \mathbf{m}_k) (\mathbf{z}_t - \mathbf{m}_k)^\top \right] \mathbf{C}_k^{-1} \Gamma \right) \\ & = \frac{1}{T} \sum_{t=1}^T 2\delta_t \xi_k \text{tr} (\mathbf{C}_k^{-1} \mathbf{B}_{tk} \mathbf{C}_k^{-1} \Gamma). \end{aligned}$$

Recall now the following identity connecting the gradient with the derivative [30, Appendix A.5]:

$$\begin{aligned} & \text{D}_{\mathbf{C}_k} \hat{\mathcal{L}}_\mu(\Omega)[\Gamma] = \langle \frac{\partial \hat{\mathcal{L}}_\mu}{\partial \mathbf{C}_k} | \Gamma \rangle_{\mathbf{C}_k} \\ \Rightarrow \frac{1}{T} \sum_{t=1}^T 2\delta_t \xi_k \text{tr} (\mathbf{C}_k^{-1} \mathbf{B}_{tk} \mathbf{C}_k^{-1} \Gamma) & = \langle \frac{\partial \hat{\mathcal{L}}_\mu}{\partial \mathbf{C}_k} | \Gamma \rangle_{\mathbf{C}_k}, \end{aligned} \quad (33)$$

where $\langle \cdot | \cdot \rangle_{\mathbf{C}_k}$ stands for the adopted Riemannian metric.

In the case of the Affl metric, (33) yields

$$\frac{1}{T} \sum_{t=1}^T 2\delta_t \xi_k \text{tr} (\mathbf{C}_k^{-1} \mathbf{B}_{tk} \mathbf{C}_k^{-1} \Gamma) = \text{tr} (\mathbf{C}_k^{-1} \frac{\partial \hat{\mathcal{L}}_\mu}{\partial \mathbf{C}_k} \mathbf{C}_k^{-1} \Gamma),$$

and because Γ was chosen arbitrarily,

$$\frac{\partial \hat{\mathcal{L}}_\mu}{\partial \mathbf{C}_k} = \frac{1}{T} \sum_{t=1}^T 2\delta_t \xi_k \mathbf{B}_{tk},$$

which establishes (18c).

In the case of the BW metric, (33) yields

$$\begin{aligned} \frac{1}{T} \sum_{t=1}^T 2\delta_t \xi_k \operatorname{tr}(\mathbf{C}_k^{-1} \mathbf{B}_{tk} \mathbf{C}_k^{-1} \Gamma) &= \frac{1}{2} \operatorname{tr}(L_{\mathbf{C}_k}(\frac{\partial \hat{\mathcal{L}}_\mu}{\partial \mathbf{C}_k}) \Gamma) \\ \Rightarrow L_{\mathbf{C}_k}(\frac{\partial \hat{\mathcal{L}}_\mu}{\partial \mathbf{C}_k}) &= \frac{1}{T} \sum_{t=1}^T 4\delta_t \xi_k \mathbf{C}_k^{-1} \mathbf{B}_{tk} \mathbf{C}_k^{-1}. \end{aligned}$$

Hence, by recalling also the definition of the Lyapunov operator from the discussion below (15),

$$\frac{\partial \hat{\mathcal{L}}_\mu}{\partial \mathbf{C}_k} = \frac{1}{T} \sum_{t=1}^T 4\delta_t \xi_k [\mathbf{C}_k^{-1} \mathbf{B}_{tk} + \mathbf{B}_{tk} \mathbf{C}_k^{-1}],$$

which establishes (18d).

APPENDIX E PROOF OF PROPOSITION 11

To conserve space, the proof that the classical Bellman mappings take $L_2(\mathfrak{P})$ into itself is omitted, as it can be obtained straightforwardly by applying elementary inequalities, such as

$$\begin{aligned} \|\mathcal{T}_\mu^\diamond Q\|_{L_2(\mathfrak{P})}^2 &\leq 2\|g\|_{L_2(\mathfrak{P})}^2 \\ &\quad + 2\alpha^2 \mathbb{E}\{|\mathbb{E}_{s'|z}\{Q(\zeta(s', \mu(s')))\}|^2\}, \end{aligned}$$

for example, to establish $\|\mathcal{T}_\mu^\diamond Q\|_{L_2(\mathfrak{P})}^2 < +\infty, \forall Q \in L_2(\mathfrak{P})$, and by mirroring arguments from the subsequent proof.

First, for any subset \mathcal{E} of Λ within the probability space $(\Lambda, \mathfrak{F}, \mathbb{P})$, define the indicator function $I_{\mathcal{E}}: \Lambda \rightarrow \{0, 1\}$ with $I_{\mathcal{E}}(\lambda) = 1$, if $\lambda \in \mathcal{E}$, while $I_{\mathcal{E}}(\lambda) = 0$, if $\lambda \notin \mathcal{E}$. Then, owing to well-known properties of the conditional expectation [40, §9.7], such as Jensen's inequality, it can be verified that $\forall Q_1, Q_2 \in L_2(\mathfrak{P})$ and with $z' := \zeta(s', \mathbf{a}')$,

$$\begin{aligned} &\|\mathcal{T}_\mu^\diamond Q_1 - \mathcal{T}_\mu^\diamond Q_2\|_{L_2(\mathfrak{P})}^2 \\ &= \alpha^2 \mathbb{E}\{|\mathbb{E}_{s'|z}\{Q_1(\zeta(s', \mu(s'))) - Q_2(\zeta(s', \mu(s')))\}|^2\} \\ &\leq \alpha^2 \mathbb{E}\mathbb{E}_{s'|z}\{ |Q_1(\zeta(s', \mu(s'))) - Q_2(\zeta(s', \mu(s')))|^2 \} \\ &= \alpha^2 \mathbb{E}\{ |Q_1(\zeta(s', \mu(s'))) - Q_2(\zeta(s', \mu(s')))|^2 \} \\ &= \alpha^2 \mathbb{E}\{ |Q_1(\zeta(s', \mathbf{a}')) - Q_2(\zeta(s', \mathbf{a}'))|^2 I_{\{\mathbf{a}' = \mu(s')\}} \} \\ &\leq \alpha^2 \mathbb{E}\{ |Q_1(\zeta(s', \mathbf{a}')) - Q_2(\zeta(s', \mathbf{a}'))|^2 \} \\ &= \alpha^2 \mathbb{E}\{ |Q_1(z') - Q_2(z')|^2 \} = \alpha^2 \|Q_1 - Q_2\|_{L_2(\mathfrak{P})}^2, \end{aligned}$$

which establishes (20a).

The following fact, taken from [15, Lemma 11], is adapted to the current setting.

Fact 15 ([15, Lemma 11]). For any $Q_1, Q_2 \in L_2(\mathfrak{P})$ and any $\mathbf{s} \in \mathfrak{S}$, there exists a $\delta(\mathbf{s}) \neq 0$ s.t. for any $\epsilon(\mathbf{s}) \in (0, \sqrt{|\delta(\mathbf{s})|})$, an $\mathbf{a}_\#(\mathbf{s}) \in \mathfrak{A}$ can be always selected with

$$\begin{aligned} &|\inf_{\bar{\mathbf{a}} \in \mathfrak{A}} Q_1(\zeta(\mathbf{s}, \bar{\mathbf{a}})) - \inf_{\bar{\mathbf{a}} \in \mathfrak{A}} Q_2(\zeta(\mathbf{s}, \bar{\mathbf{a}}))|^2 \\ &\leq |Q_1(\zeta(\mathbf{s}, \mathbf{a}_\#(\mathbf{s}))) - Q_2(\zeta(\mathbf{s}, \mathbf{a}_\#(\mathbf{s})))|^2 + \epsilon(\mathbf{s}). \quad (34) \end{aligned}$$

According to Fact 15, for arbitrarily fixed $Q_1, Q_2 \in L_2(\mathfrak{P})$, $\epsilon \in \mathbb{R}_{++}$, and $\mathbf{s} \in \mathfrak{S}$, choose any $\epsilon(\mathbf{s}) \in$

$(0, \min\{\epsilon/\alpha^2, \sqrt{|\delta(\mathbf{s})|}\})$ together with its associated $\mathbf{a}_\#(\mathbf{s})$ which satisfies (34). Then, by applying Jensen's inequality again,

$$\begin{aligned} &\|\mathcal{T}^\diamond Q_1 - \mathcal{T}^\diamond Q_2\|_{L_2(\mathfrak{P})}^2 \\ &\leq \alpha^2 \mathbb{E}\mathbb{E}_{s'|z}\{|\inf_{\bar{\mathbf{a}} \in \mathfrak{A}} Q_1(z(s', \bar{\mathbf{a}})) - \inf_{\bar{\mathbf{a}} \in \mathfrak{A}} Q_2(z(s', \bar{\mathbf{a}}))|^2\} \\ &= \alpha^2 \mathbb{E}\{|\inf_{\bar{\mathbf{a}} \in \mathfrak{A}} Q_1(z(s', \bar{\mathbf{a}})) - \inf_{\bar{\mathbf{a}} \in \mathfrak{A}} Q_2(z(s', \bar{\mathbf{a}}))|^2\} \\ &\leq \alpha^2 \mathbb{E}\{ |Q_1(z(s', \mathbf{a}_\#(s'))) - Q_2(z(s', \mathbf{a}_\#(s')))|^2 \} \\ &\quad + \alpha^2 \mathbb{E}\{\epsilon(s')\} \\ &= \alpha^2 \mathbb{E}\{ |Q_1(z(s', \mathbf{a}')) - Q_2(z(s', \mathbf{a}'))|^2 I_{\{\mathbf{a}' = \mathbf{a}_\#(s')\}} \} \\ &\quad + \alpha^2 \mathbb{E}\{\epsilon(s')\} \\ &\leq \alpha^2 \mathbb{E}\{ |Q_1(z') - Q_2(z')|^2 \} + \alpha^2 \mathbb{E}\{\frac{\epsilon}{\alpha^2}\} \\ &= \alpha^2 \|Q_1 - Q_2\|_{L_2(\mathfrak{P})}^2 + \epsilon, \end{aligned}$$

which establishes (20b) because ϵ is an arbitrarily chosen positive real number.

APPENDIX F PROOF OF LEMMA 12

According to basic properties of the conditional expectation [40, §9.7],

$$\begin{aligned} \mathcal{L}_\mu(Q) &= \alpha^2 \mathbb{E}\{ [Q(z') - \mathbb{E}_{s'|z}\{Q(z')\}]^2 \} \\ &\quad + \mathbb{E}\{ [g(z) + \alpha \mathbb{E}_{s'|z}\{Q(z')\} - Q(z)]^2 \} \\ &\quad + 2\alpha \mathbb{E}\{ [g(z) + \alpha \mathbb{E}_{s'|z}\{Q(z')\} - Q(z)] \\ &\quad \quad \cdot [Q(z') - \mathbb{E}_{s'|z}\{Q(z')\}] \} \\ &\quad \quad \quad \mathbb{V}_{s'|z}\{Q(z')\} \\ &= \alpha^2 \mathbb{E}\{ \overbrace{\mathbb{E}_{s'|z}\{ [Q(z') - \mathbb{E}_{s'|z}\{Q(z')\}]^2 \}} \} \\ &\quad + \mathbb{E}\{ [g(z) + \alpha \mathbb{E}_{s'|z}\{Q(z')\} - Q(z)]^2 \} \\ &\quad + 2\alpha \mathbb{E}\mathbb{E}_{s'|z}\{ [g(z) + \alpha \mathbb{E}_{s'|z}\{Q(z')\} - Q(z)] \\ &\quad \quad \cdot [Q(z') - \mathbb{E}_{s'|z}\{Q(z')\}] \} \\ &= \alpha^2 \mathbb{E}\{ \mathbb{V}_{z'|z}\{Q(z')\} \} + \|Q - \mathcal{T}_\mu^\diamond Q\|_{L_2(\mathfrak{P})}^2 \\ &\quad + 2\alpha \mathbb{E}\{ [g(z) + \alpha \mathbb{E}_{s'|z}\{Q(z')\} - Q(z)] \\ &\quad \quad \cdot \mathbb{E}_{s'|z}\{Q(z') - \mathbb{E}_{s'|z}\{Q(z')\}\} \} \\ &= \alpha^2 \mathbb{E}\{ \mathbb{V}_{s'|z}\{Q(z')\} \} + \|Q - \mathcal{T}_\mu^\diamond Q\|_{L_2(\mathfrak{P})}^2. \end{aligned}$$

This establishes Lemma 12.

APPENDIX G PROOF OF PROPOSITION 14

A. Proof of Proposition 14(i)

For any n , any $\epsilon \in (0, \delta_\circ]$, and according to [42, Thm. 3.14, pp. 69], there exists $\tilde{Q} \in C(\mathfrak{Z})$ s.t. $\|Q_{\mu_n}^\diamond - \tilde{Q}\|_{L_2(\mathfrak{P})} \leq \epsilon$. Then, by employing also Proposition 11,

$$\begin{aligned} &\|\tilde{Q} - \mathcal{T}_{\mu_n}^\diamond \tilde{Q}\|_{L_2(\mathfrak{P})} \\ &= \|\tilde{Q} - \mathcal{T}_{\mu_n}^\diamond \tilde{Q} - (Q_{\mu_n}^\diamond - \mathcal{T}_{\mu_n}^\diamond Q_{\mu_n}^\diamond)\|_{L_2(\mathfrak{P})} \\ &\leq \|\tilde{Q} - Q_{\mu_n}^\diamond\|_{L_2(\mathfrak{P})} + \|\mathcal{T}_{\mu_n}^\diamond Q_{\mu_n}^\diamond - \mathcal{T}_{\mu_n}^\diamond \tilde{Q}\|_{L_2(\mathfrak{P})} \\ &\leq (1 + \alpha) \|\tilde{Q} - Q_{\mu_n}^\diamond\|_{L_2(\mathfrak{P})} \\ &\leq (1 + \alpha)\epsilon. \end{aligned}$$

Moreover, by Lemma 12, with $z' = \zeta(s', \mu_n(s'))$,

$$\begin{aligned} & \|Q_n - \mathcal{T}_{\mu_n}^\diamond Q_n\|_{L_2(\mathfrak{P})}^2 \\ &= \mathcal{L}_{\mu_n}(Q_n) - \alpha^2 \mathbb{E}\{\mathbb{V}_{s'|z}\{Q_n(z')\}\} \leq \mathcal{L}_{\mu_n}(Q_n) \\ &\leq \hat{\mathcal{L}}_{\mu_n}[T](Q_n) + \delta_{\mathfrak{E}_\sharp} \end{aligned} \quad (35a)$$

$$\leq \inf_{Q \in \mathcal{Q}_K} \hat{\mathcal{L}}_{\mu_n}[T](Q) + \Delta + \delta_{\mathfrak{E}_\sharp} \quad (35b)$$

$$\leq \inf_{Q \in \cup_{K \in \mathbb{N}_*} \mathcal{Q}_K} \hat{\mathcal{L}}_{\mu_n}[T](Q) + \delta_{\text{inf}} + \Delta + \delta_{\mathfrak{E}_\sharp} \quad (35c)$$

$$= \inf_{Q \in C(3)} \hat{\mathcal{L}}_{\mu_n}[T](Q) + \delta_{\text{inf}} + \Delta + \delta_{\mathfrak{E}_\sharp} \quad (35d)$$

$$\leq \hat{\mathcal{L}}_{\mu_n}[T](\tilde{Q}) + \delta_{\text{inf}} + \Delta + \delta_{\mathfrak{E}_\sharp} \quad (35e)$$

$$\leq \mathcal{L}_{\mu_n}(\tilde{Q}) + \delta_{\text{inf}} + \Delta + 2\delta_{\mathfrak{E}_\sharp} \quad (35f)$$

$$\begin{aligned} &= \|\tilde{Q} - \mathcal{T}_{\mu_n}^\diamond \tilde{Q}\|_{L_2(\mathfrak{P})}^2 + \alpha^2 \mathbb{E}\{\mathbb{V}_{s'|z}\{\tilde{Q}(z')\}\} \\ &\quad + \delta_{\text{inf}} + \Delta + 2\delta_{\mathfrak{E}_\sharp} \\ &\leq (1 + \alpha)^2 \epsilon^2 + \alpha^2 \mathbb{E}\{\mathbb{V}_{s'|z}\{\tilde{Q}(z')\}\} \\ &\quad + \delta_{\text{inf}} + \Delta + 2\delta_{\mathfrak{E}_\sharp} \\ &\leq (1 + \alpha)^2 \epsilon^2 + \alpha^2 \sigma_{\mathbb{V}}^2 + \delta_{\text{inf}} + \Delta + 2\delta_{\mathfrak{E}_\sharp}, \end{aligned} \quad (35g)$$

where Assumption 13(i) was used in (35a) and (35e), Assumption 13(ii) was used in (35b), Assumption 13(iii) in (35c), Proposition 4 in (35d), Lemma 12 in (35f), and Assumption 13(iv) in (35g). Further, by Proposition 11,

$$\begin{aligned} & \|Q_n - Q_{\mu_n}^\diamond\|_{L_2(\mathfrak{P})} \\ &\leq \|Q_n - \mathcal{T}_{\mu_n}^\diamond Q_n\|_{L_2(\mathfrak{P})} + \|\mathcal{T}_{\mu_n}^\diamond Q_n - \mathcal{T}_{\mu_n}^\diamond Q_{\mu_n}^\diamond\|_{L_2(\mathfrak{P})} \\ &\leq ((1 + \alpha)^2 \epsilon^2 + \alpha^2 \sigma_{\mathbb{V}}^2 + \delta_{\text{inf}} + \Delta + 2\delta_{\mathfrak{E}_\sharp})^{1/2} \\ &\quad + \alpha \|Q_n - Q_{\mu_n}^\diamond\|_{L_2(\mathfrak{P})}, \end{aligned}$$

and thus, because ϵ was chosen arbitrarily,

$$\|Q_n - Q_{\mu_n}^\diamond\|_{L_2(\mathfrak{P})} \leq \frac{\sqrt{\alpha^2 \sigma_{\mathbb{V}}^2 + \delta_{\text{inf}} + \Delta + 2\delta_{\mathfrak{E}_\sharp}}}{1 - \alpha},$$

$\forall n$, which establishes Proposition 14(i).

B. Proof of Proposition 14(ii)

The following auxiliary lemma is first in order.

Lemma 16. For sufficiently large n ,

$$\begin{aligned} \|Q_{\mu_{n+1}}^\diamond - Q^\diamond\|_{L_2(\mathfrak{P})} &\leq \alpha \|Q_{\mu_n}^\diamond - Q^\diamond\|_{L_2(\mathfrak{P})} \\ &\quad + \alpha(2\Delta_1 + \Delta_2). \end{aligned}$$

Proof. Note that under the greedy policy improvement $\mu_{n+1}(\mathbf{s}) := \arg \min_{\mathbf{a} \in \mathfrak{A}} Q_n(\zeta(\mathbf{s}, \mathbf{a})) \Rightarrow Q_n(\zeta(\mathbf{s}, \mu_{n+1}(\mathbf{s}))) = \min_{\mathbf{a} \in \mathfrak{A}} Q_n(\zeta(\mathbf{s}, \mathbf{a}))$, so that by (1),

$$\mathcal{T}^\diamond Q_n = \mathcal{T}_{\mu_{n+1}}^\diamond Q_n. \quad (36)$$

Then, the claim of Lemma 16 can be established as follows,

$$\begin{aligned} & \|Q_{\mu_{n+1}}^\diamond - Q^\diamond\|_{L_2(\mathfrak{P})} \\ &\leq \|Q_{\mu_{n+1}}^\diamond - \mathcal{T}^\diamond Q_n\|_{L_2(\mathfrak{P})} + \|\mathcal{T}^\diamond Q_n - Q^\diamond\|_{L_2(\mathfrak{P})} \\ &= \|Q_{\mu_{n+1}}^\diamond - \mathcal{T}^\diamond Q_n\|_{L_2(\mathfrak{P})} + \|\mathcal{T}^\diamond Q_n - \mathcal{T}^\diamond Q^\diamond\|_{L_2(\mathfrak{P})} \\ &\leq \|Q_{\mu_{n+1}}^\diamond - \mathcal{T}^\diamond Q_n\|_{L_2(\mathfrak{P})} + \alpha \|Q_n - Q^\diamond\|_{L_2(\mathfrak{P})} \quad (37a) \\ &\leq \|Q_{\mu_{n+1}}^\diamond - \mathcal{T}^\diamond Q_n\|_{L_2(\mathfrak{P})} + \alpha \|Q_n - Q_{\mu_n}^\diamond\|_{L_2(\mathfrak{P})} \\ &\quad + \alpha \|Q_{\mu_n}^\diamond - Q^\diamond\|_{L_2(\mathfrak{P})} \end{aligned}$$

$$\leq \alpha \|Q_{\mu_n}^\diamond - Q^\diamond\|_{L_2(\mathfrak{P})} + \alpha \Delta_1 + \|Q_{\mu_{n+1}}^\diamond - \mathcal{T}^\diamond Q_n\|_{L_2(\mathfrak{P})} \quad (37b)$$

$$\begin{aligned} &\leq \alpha \|Q_{\mu_n}^\diamond - Q^\diamond\|_{L_2(\mathfrak{P})} + \alpha \Delta_1 \\ &\quad + \|Q_{\mu_{n+1}}^\diamond - \mathcal{T}_{\mu_{n+1}}^\diamond Q_{\mu_n}^\diamond\|_{L_2(\mathfrak{P})} \\ &\quad + \|\mathcal{T}_{\mu_{n+1}}^\diamond Q_{\mu_n}^\diamond - \mathcal{T}_{\mu_{n+1}}^\diamond Q_n\|_{L_2(\mathfrak{P})} \\ &\quad + \|\mathcal{T}_{\mu_{n+1}}^\diamond Q_n - \mathcal{T}^\diamond Q_n\|_{L_2(\mathfrak{P})} \\ &= \alpha \|Q_{\mu_n}^\diamond - Q^\diamond\|_{L_2(\mathfrak{P})} + \alpha \Delta_1 \\ &\quad + \|\mathcal{T}_{\mu_{n+1}}^\diamond Q_{\mu_{n+1}}^\diamond - \mathcal{T}_{\mu_{n+1}}^\diamond Q_{\mu_n}^\diamond\|_{L_2(\mathfrak{P})} \\ &\quad + \|\mathcal{T}_{\mu_{n+1}}^\diamond Q_{\mu_n}^\diamond - \mathcal{T}_{\mu_{n+1}}^\diamond Q_n\|_{L_2(\mathfrak{P})} \\ &\quad + \|\mathcal{T}_{\mu_{n+1}}^\diamond Q_n - \mathcal{T}^\diamond Q_n\|_{L_2(\mathfrak{P})} \\ &\leq \alpha \|Q_{\mu_n}^\diamond - Q^\diamond\|_{L_2(\mathfrak{P})} + \alpha \Delta_1 + \alpha \|Q_{\mu_{n+1}}^\diamond - Q_{\mu_n}^\diamond\|_{L_2(\mathfrak{P})} \\ &\quad + \alpha \|Q_{\mu_n}^\diamond - Q_n\|_{L_2(\mathfrak{P})} \end{aligned} \quad (37c)$$

$$\leq \alpha \|Q_{\mu_n}^\diamond - Q^\diamond\|_{L_2(\mathfrak{P})} + \alpha(2\Delta_1 + \Delta_2), \quad (37d)$$

where Proposition 11 was used in (37a) and (37c), Proposition 14(i) in (37b) and (37d), while (36) and Assumption 13(v) were utilized in (37d). \square

For sufficiently large n , application of Lemma 16 for an arbitrarily fixed $I \in \mathbb{N}_*$ number of times yields

$$\begin{aligned} & \|Q_{\mu_{n+I}}^\diamond - Q^\diamond\|_{L_2(\mathfrak{P})} \\ &\leq \alpha^I \|Q_{\mu_n}^\diamond - Q^\diamond\|_{L_2(\mathfrak{P})} + \sum_{i=0}^{I-1} \alpha^{i+1} (2\Delta_1 + \Delta_2) \\ &\leq \alpha^I \|Q_{\mu_n}^\diamond - Q^\diamond\|_{L_2(\mathfrak{P})} + \underbrace{\frac{\alpha}{1-\alpha} (2\Delta_1 + \Delta_2)}_{\Delta'}. \end{aligned}$$

Because of $\alpha \in [0, 1)$,

$$\begin{aligned} & \limsup_{n \rightarrow \infty} \|Q_{\mu_n}^\diamond - Q^\diamond\|_{L_2(\mathfrak{P})} \\ &= \limsup_{I \rightarrow \infty} \|Q_{\mu_{n+I}}^\diamond - Q^\diamond\|_{L_2(\mathfrak{P})} \leq \Delta'. \end{aligned}$$

Now, the triangle inequality and Proposition 14(i) suggest

$$\begin{aligned} & \|Q_n - Q^\diamond\|_{L_2(\mathfrak{P})} \\ &\leq \|Q_n - Q_{\mu_n}^\diamond\|_{L_2(\mathfrak{P})} + \|Q_{\mu_n}^\diamond - Q^\diamond\|_{L_2(\mathfrak{P})} \\ &\leq \Delta_1 + \|Q_{\mu_n}^\diamond - Q^\diamond\|_{L_2(\mathfrak{P})}. \end{aligned}$$

An application of $\limsup_{n \rightarrow \infty}$ to the previous inequality establishes Proposition 14(ii).